ELECTROMAGNETICS LABORATORY
TECHNICAL REPORT NO. 84-13

July 1984

WAVE ATTENUATION AND MODE DISPERSION IN A WAVEGUIDE COATED WITH LOSSY DIELECTRIC MATERIAL

C. S. Lee
S. L. Chuang
S. W. Lee
Y. T. Lo

Supported by
Grant NAG3-475
NASA-Lewis Research Center
Cleveland, Ohio 44135

ELECTROMAGNETICS LABORATORY
DEPARTMENT OF ELECTRICAL AND COMPUTER ENGINEERING
ENGINEERING EXPERIMENT STATION
UNIVERSITY OF ILLINOIS AT URBANA-CHAMPAIGN
URBANA, ILLINOIS 61801

UILU-ENG-84-2552

Electromagnetics Laboratory Report No. 84-13

WAVE ATTENUATION AND MODE DISPERSION IN A WAVEGUIDE COATED WITH LOSSY DIELECTRIC MATERIAL

by

C. S. Lee, S. L. Chuang, S. W. Lee and Y. T. Lo

Technical Report

July 1984

Supported by

Grant No. NAG3-475
NASA-Lewis Research Center
Cleveland, Ohio 44135

Electromagnetics Laboratory
Department of Electrical and Computer Engineering
Engineering Experiment Station
University of Illinois at Urbana-Champaign
Urbana, Illinois 61801

ABSTRACT

The modal attenuation constants in a cylindrical waveguide coated with a lossy dielectric material are studied as functions of frequency, dielectric constant, and thickness of the dielectric layer. A dielectric material best suited for a large attenuation is suggested. Using Kirchhoff's approximation, we also studied the field attenuation in a coated waveguide, which is illuminated by a normally incident plane wave. For a circular guide which has a diameter of 2 wavelengths and is coated with a thin lossy dielectric layer ($\varepsilon_r = 9.1 - j2.3$, thickness = 3% of the radius), a 3 dB attenuation is achieved within 16 diameters.

TABLE OF CONTENTS

LIST OF FIGURES

Figure | Page

LIST OF SYMBOLS

a,b	Inner and outer radii of the partially filled cylinder (Figure 1).
A,B,C,D	Constants (Equations A2.1 through A2.4).
$\vec{A},\vec{F}$	Magnetic and electric vector potentials (Equations A1.1, A1.2).
$C_{mn}^{H,\nu}, \overline{C}_{mn}^{H,\nu}$	Constants (Equations A3.15, A3.16).
$\vec{E},\vec{H}$	Electric and magnetic fields.
E_ϕ,E_ρ,E_z	Components of the electric field in a cylindrical coordinate.
H_ϕ,H_ρ,H_z	Components of the magnetic field in a cylindrical coordinate.
E_o	Magnitude of the incident electric field.
$\vec{E}^{in},\vec{H}^{in}$	Incident fields.
f	Frequency.
$f_m(x)$	(Equation 2.4).
$F_1,F_1',F_3,F_3',F_4,F_4'$	(Equations 2.8 - 2.14).
HE,EH	Hybrid modes corresponding to TE and TM modes.
J_m,N_m	Bessel and Neumann functions of order m.
k	Wave number.
k_o	Free-space wave number ($= \omega\sqrt{\mu_o \varepsilon_o}$)
k_x,k_z	Components of the wave vector in a rectangular coordinate.
$k_\rho,k_{\rho o}$	Radial wave vectors of the normal modes in the perturbed and unperturbed cylindrical waveguides.
k_z,k_{zo}	z-components of the wave vectors of the normal modes in the perturbed and unperturbed cylindrical waveguides.
$N_{mn},\overline{N}_{mn}$	Normalization constants (Equations A3.9, A3.10).
P_o	Incident power on the area of the aperture of a cylindrical waveguide from a normally incident field (Equation A3.20).
$P(z)$	Power of the waves in the waveguide (Equation A3.20).

TE,TM	Transverse electric and transverse magnetic fields.
$\dot{Y}$	(Equation A3.14)
$\dot{U}_{mn}^{V,H}, \dot{V}_{mn}^{V,H}$	Normalized TE and TM fields (Equations 2.26, 2.27).
Z_o	Free-space impedance ($= \sqrt{\mu_o/\varepsilon_o}$).
α, α_{mn}	Attenuation constants.
β_{mn}	Real part of propagation constant.
ε_r	Dielectric constant.
$\varepsilon_r^R, \varepsilon_r^I$	Real and imaginary parts of the dielectric constant.
θ_o	Incident angle (Figure 2).
μ, ε	Permeability and permittivity constants.
$\mu_o, \varepsilon_o,$	Permeability and permittivity constants in free space.
ξ_{mn}, ξ'_{mn}	Zeros of $J_{mn}(x)$ and $J'_{mn}(x)$.
$\hat{\rho}, \hat{\phi}, \hat{z}$	Unit vectors in a cylindrical coordinate.
τ	Thickness of the dielectric layer, b - a (Figure 1).
$\psi, \overline{\psi}$	Wave functions for TE and TM modes.
ω	Angular frequency.
Subscript t	Transverse.
Subscripts H,V	Horizontal and vertical polarizations.
Subscripts m,n	Angular and radial indices.
Subscripts ρ, ϕ, z	Components in a cylindrical coordinate.
Subscripts 1,2	Regions I and II (Figure 1).
Superscripts I,II	Regions I and II (Figure 1).
bar, without bar	TE, TM (e.g., $\psi, \overline{\psi}$).

1. INTRODUCTION

Reducing the radar cross section (RCS) is one of the major problems in designing a modern military aircraft. When an airplane is heading toward the radar site, a major contribution to RCS comes from the jet engine intake. The RCS from the jet intake is mainly due to the rim diffraction and interior irradiation. The rim diffraction has been studied by several authors [1], [2].

The main goal of our research is to reduce, as much as possible, the interior irradiation from the jet intake. One way to achieve this goal is to coat the interior wall of the jet intake with a lossy dielectric material. Once the wave is transmitted from the outside illumination, the wave will attenuate as it propagates through the interior of the jet intake before it scatters back to the outside of the jet intake.

For our theoretical model, we approximate the jet intake by a cylindrical waveguide. We will investigate the properties of the wave attenuation in a cylindrical waveguide coated with a lossy dielectric material and suggest how the power attenuation of the transmitted wave to the waveguide from the outside illumination can be maximized.

This report begins with the derivation of the normal modes in the lossy waveguide. It is followed by the general discussion of the behavior of the attenuation constant as functions of the frequency, the dielectric constant and the layer thickness of the dielectric material. A few specific materials are chosen to show how the wave attenuates within the waveguide from the normally incident plane wave. In the conclusion and discussion section, other possible devices for a large power attenuation of the wave are suggested.

2. FORMULATION

Consider a cylindrical waveguide coated with a lossy material as shown in Figure 1. We assume that region I is free space and the permeability of region II is the same as that in free space. In the past, a number of authors treated the problem of the partially filled waveguide [3], [4]. In this report, we rederive the formulation to make this report self-sufficient and uniform in notation for other derivations presented later.

2.1. Propagation Constant

2.1.1. Approximate solution

Though the perturbation theory does not give a very accurate result for the waveguide perturbed by a very lossy material, this analytic result provides guidance in the exact numerical calculation.

The difference between the propagation constants of the perturbed and unperturbed waveguides is given by ($e^{j\omega t}$ convention)[5]

$$k_z - k_{zo} = \frac{\omega \int_S (\Delta\mu \vec{H}\cdot\vec{H}_o - \Delta\varepsilon \vec{E}\cdot\vec{E}_o)\, dS}{\int_S (\vec{E}_o \times \vec{H} - \vec{E} \times \vec{H}_o)\cdot\hat{z}\, dS} \tag{2.1}$$

Here $\vec{E}(\vec{H})$ and $\vec{E}_o(\vec{H}_o)$ are the fields of the perturbed and unperturbed waveguides, respectively, ω is the angular frequency, and $\Delta\mu$ and $\Delta\varepsilon$ are the differences of the permeabilities and permittivities between the perturbed and unperturbed cases, respectively. The integration is over the cross-sectional area of the waveguide. In this report, we assume that $\Delta\mu = 0$ and $\Delta\varepsilon = (\varepsilon_r - 1)\varepsilon_o$ where ε_o is the free-space permittivity and ε_r is the dielectric constant of the lossy dielectric.

In the cylindrically symmetric geometry, mode coupling is largest between the TE and TM modes with the same mode indices, e.g., TE_{11} and TM_{11}. Though the normal mode in this case is no longer TE or TM, it is closer to one of the two modes when the thickness of the dielectric layer is small. We call this mode "quasi" TE or TM mode and will use the same notation as in the unperturbed waveguide for convenience. Some authors prefer to use HE and EH instead of TE and TM, respectively[4].

Using the static approximation, we obtain (Appendix 1)

$$k_z - k_{zo} = \frac{\omega^2 \mu_o \varepsilon_o (\varepsilon_r - 1)}{2 \varepsilon_r k_{zo}} \left\{ 1 - \frac{f_m\left(\frac{\xi'_{mn} a}{b}\right)}{\frac{(\xi'_{mn})^2 - n^2}{2} J_m^2(\xi'_{mn})} \right\} \quad \text{for } TE_{mn}(HE_{mn}) \qquad (2.2)$$

$$k_z - k_{zo} = \frac{k_{zo}(\varepsilon_r - 1)}{2\varepsilon_r} \left\{ 1 - \frac{f_m\left(\frac{\xi_{mn} a}{b}\right)}{\frac{\xi_{mn}^2}{2} J_{m+1}^2(\xi_{mn})} \right\} \quad \text{for } TM_{mn}(EH_{mn}) \qquad (2.3)$$

Here μ_o is the free-space permeability; ξ_{mn} and ξ'_{mn} are the n^{th} zeros of the Bessel function of order m, J_m and its derivative J'_m, respectively; $k_{\rho o}$ is the radial wave vector for the unperturbed case; and

$$f_m(x) = \frac{x^2}{2} \left[J_{m+1}^2(x) - J_m(x) J_{m+1}(x) \right] + m J_m^2(x) \qquad (2.4)$$

2.1.2. Exact solution

The characteristic equation for the propagation constant of the normal mode in a lossy hollow cylinder can be derived by imposing the boundary condition on the perfectly conducting surface and matching the fields between regions I and II (Figure 1). The characteristic equation to be solved numerically for the propagation constant k_z is given by (Appendix 2)

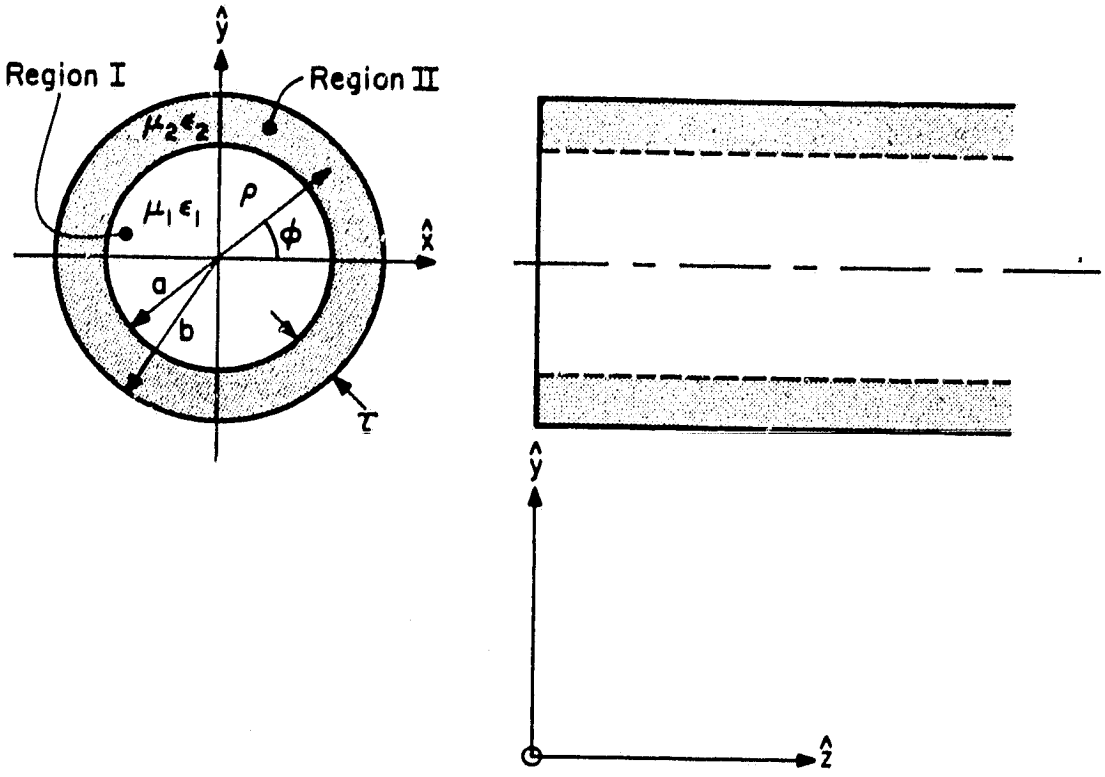

Figure 1. A cylindrical waveguide coated with a dielectric material.

$$k_{\rho 1}^2\left(F_1' - \frac{\varepsilon_2}{\varepsilon_1}\frac{F_3' F_1}{F_3}\frac{k_{\rho 1}}{k_{\rho 2}}\right)\left(F_1' - \frac{\mu_2}{\mu_1}\frac{F_1 F_4'}{F_4}\frac{k_{\rho 1}}{k_{\rho 2}}\right) - \left(\frac{k_z m}{\omega a}\right)^2 \frac{1}{\varepsilon_1 \mu_1} F_1^2 \left(1 - \frac{k_{\rho 1}^2}{k_{\rho 2}^2}\right)^2 = 0 \tag{2.5}$$

where

$$k_{\rho 1}^2 + k_z^2 = \omega^2 \varepsilon_1 \mu_1 \equiv k_1^2 \tag{2.6}$$

$$k_{\rho 2}^2 + k_z^2 = \omega^2 \varepsilon_2 \mu_2 \equiv k_2^2 \tag{2.7}$$

$$F_1 = J_m(k_{\rho 1} a) \tag{2.8}$$

$$F_3 = J_m(k_{\rho 2} a)\, N_m(k_{\rho 2} b) - N_m(k_{\rho 2} a)\, J_m(k_{\rho 2} b) \tag{2.9}$$

$$F_3' = J_m'(k_{\rho 2} a)\, N_m(k_{\rho 2} b) - N_m'(k_{\rho 2} a)\, J_m(k_{\rho 2} b) \tag{2.10}$$

$$F_4 = J_m(k_{\rho 2} a)\, N_m'(k_{\rho 2} b) - N_m(k_{\rho 2} a)\, J_m'(k_{\rho 2} b) \tag{2.11}$$

$$F_4' = J_m'(k_{\rho 2} a)\, N_m'(k_{\rho 2} b) - N_m'(k_{\rho 2} a)\, J_m'(k_{\rho 2} b) \tag{2.12}$$

Here ε_1 and ε_2 are the permittivities; μ_2 and μ_1, the permeabilities; $k_{\rho 1}$ and $k_{\rho 2}$, the radial wave vectors of regions I and II, respectively; and a and b are the radii of the air region and the conducting cylinder, respectively. J_m is the Bessel function and N_m is the Neumann function of order m.

2.2. Fields of the Normal Modes in a Lossy Waveguide

Once we find the eigenvalues for the propagation constants, the eigenvectors for the fields in the lossy waveguide naturally follow. The electric and magnetic fields are given by (Appendix 2)

$$E_\rho^I = \left[-\frac{A k_z k_{\rho 1}}{\omega \varepsilon_1} J_m'(k_{\rho 1}\rho) - \frac{Bm}{\rho} J_m(k_{\rho 1}\rho)\right] \cos m\phi\, e^{-jk_z z} \tag{2.13a}$$

$$E_\rho^{II} = \left[-\frac{Ck_z k_{\rho 2}}{\omega \varepsilon_2} \{ J_m'(k_{\rho 2}\rho)\, N_m(k_{\rho 2}b) - N_m'(k_{\rho 2}\rho)\, J_m(k_{\rho 2}b) \} \right.$$

$$\left. - \frac{Dm}{\rho} \{ J_m(k_{\rho 2}\rho)\, N_m'(k_{\rho 2}b) - N_m(k_{\rho 2}\rho)\, J_m'(k_{\rho 2}b) \} \right] \cos m\phi\, e^{-jk_z z} \qquad (2.13b)$$

$$E_\phi^I = \left[\frac{Ak_z m}{\omega \varepsilon_1 \rho} J_m(k_{\rho 1}\rho) + Bk_{\rho 1} J_m'(k_{\rho 1}\rho) \right] \sin m\phi\, e^{-jk_z z} \qquad (2.14a)$$

$$E_\phi^{II} = \left[\frac{Ck_z m}{\omega \varepsilon_2 \rho} \{ J_m(k_{\rho 2}\rho)\, N_m(k_{\rho 2}b) - N_m(k_{\rho 2}\rho)\, J_m(k_{\rho 2}b) \} \right.$$

$$\left. + Dk_{\rho 2} \{ J_m'(k_{\rho 2}\rho)\, N_m'(k_{\rho 2}b) - N_m'(k_{\rho 2}\rho)\, J_m'(k_{\rho 2}b) \} \right] \sin m\phi\, e^{-jk_z z} \qquad (2.14b)$$

$$E_z^I = \frac{Ak_{\rho 1}^2}{j\omega \varepsilon_1} J_m(k_{\rho 1}\rho) \cos m\phi\, e^{-jk_z z} \qquad (2.15a)$$

$$E_z^{II} = \frac{Ck_{\rho 2}^2}{j\omega \varepsilon_2} [J_m(k_{\rho 2}\rho)\, N_m(k_{\rho 2}b) - N_m(k_{\rho 2}\rho)\, J_m(k_{\rho 2}b)] \cos m\phi\, e^{-jk_z z} \qquad (2.15b)$$

$$H_\rho^I = \left[-\frac{Am}{\rho} J_m(k_{\rho 1}\rho) - \frac{Bk_z k_{\rho 1}}{\omega \mu_1} J_m'(k_{\rho 1}\rho) \right] \sin m\phi\, e^{-jk_z z} \qquad (2.16a)$$

$$H_\rho^{II} = \left[-\frac{Cm}{\rho} \{ J_m(k_{\rho 2}\rho)\, N_m(k_{\rho 2}b) - N_m(k_{\rho 2}\rho)\, J_m(k_{\rho 2}b) \} \right.$$

$$\left. - \frac{Dk_z k_{\rho 2}}{\omega \mu_2} \{ J_m'(k_{\rho 2}\rho)\, N_m'(k_{\rho 2}b) - N_m'(k_{\rho 2}\rho)\, J_m'(k_{\rho 2}b) \} \right] \sin m\phi\, e^{-jk_z z} \qquad (2.16b)$$

$$H_\phi^I = \left[-Ak_{\rho 1} J_m'(k_{\rho 1}\rho) - \frac{Bk_z m}{\omega \mu_1 \rho} J_m(k_{\rho 1}\rho) \right] \cos m\phi\, e^{-jk_z z} \qquad (2.17a)$$

$$H_\phi^{II} = \left[-Ck_{\rho 2} \left\{ J_m'(k_{\rho 2}\rho)\, N_m(k_{\rho 2}b) - N_m'(k_{\rho 2}\rho)\, J_m(k_{\rho 2}b) \right\} - \frac{Dk_z m}{\omega \mu_2 \rho} \left\{ J_m(k_{\rho 2}\rho)\, N_m'(k_{\rho 2}b) - N_m(k_{\rho 2}\rho)\, J_m'(k_{\rho 2}b) \right\} \right] \cos m\phi\, e^{-jk_z z} \quad (2.17b)$$

$$H_z^I = \frac{Bk_{\rho 1}^2}{j\omega\mu_1} J_m(k_{\rho 2}\rho) \sin m\phi\, e^{-jk_z z} \quad (2.18a)$$

$$H_z^{II} = \frac{Dk_{\rho 2}^2}{j\omega\mu_2} \left[J_m(k_{\rho 2}\rho)\, N_m'(k_{\rho 2}b) - N_m(k_{\rho 2}\rho)\, J_m'(k_{\rho 2}b) \right] \sin m\phi\, e^{-jk_z z} \quad (2.18b)$$

Here the superscipts I and II indicate regions I and II (Figure 1), and subscripts ρ, ϕ and z indicate the radial, angular and propagation-directional components of the fields, respectively. A, B, C and D are the constants, which are determined by the boundary conditions and the normalization condition. Those constants are related by

$$C = A \frac{k_{\rho 1}^2}{k_{\rho 2}^2} \frac{F_1}{F_3} \frac{\varepsilon_2}{\varepsilon_1} \quad (2.19)$$

$$D = B \frac{k_{\rho 1}^2}{k_{\rho 2}^2} \frac{F_1}{F_4} \frac{\mu_2}{\mu_1} \quad (2.20)$$

$$\frac{B}{A} = - \frac{k_{\rho 1} \left(F_1' - \frac{\varepsilon_2}{\varepsilon_1} \frac{F_3' F_1}{F_3} \frac{k_{\rho 1}}{k_{\rho 2}} \right)}{\frac{k_z m}{\omega a \mu_1} F_2 \left(1 - \frac{k_{\rho 1}^2}{k_{\rho 2}^2} \right)} \ll 1 \quad \text{for TM(EH), } m \neq 0 \quad (2.21a)$$

$$\frac{A}{B} = -\frac{k_{\rho 1}\left(F_1' - \frac{\mu_2}{\mu_1}\frac{F_1 F_4'}{F_4}\frac{k_{\rho 1}}{k_{\rho 2}}\right)}{\frac{k_z m}{\omega a \varepsilon_1} F_1\left(1 - \frac{k_{\rho 1}^2}{k_{\rho 2}^2}\right)} \ll 1 \quad \text{for TE(HE), } m \neq 0 \tag{2.21b}$$

There is no mode coupling between the TE and TM modes for m = 0. We note that there are two degenerate modes for each angular mode index m except when m = 0. In the expressions of the fields, we have arbitrarily chosen one of those two modes.

2.3. Wave Propagation into a Cylindrical Waveguide from the Incident Plane Wave

Consider a plane wave incident on the opening of a cylindrical waveguide (Figure 2). An exact solution for the cylindrical waveguide without the dielectric coating has been derived by Weinstein [6] using the Wiener-Hopf Method. GTD has been applied by several authors [2], [7]. When the waveguide is coated with lossy material, the problem is much more complicated. Since we emphasize the wave attenuation within the waveguide, we use Kirchhoff's approximation. This method provides an approximate solution and is much simpler than the GTD or Wiener-Hopf Method.

We assume in the following derivation that the perturbation within the waveguide is weak enough so that the modal fields in the perturbed waveguide can be approximated by the modal fields in the unperturbed waveguide.

For the incident fields, we write (Figure 2)

$$\vec{E}^{in} = E_o(\hat{x}\cos\theta_o - \hat{z}\sin\theta_o)\exp[-j(k_x x + k_z z)] \tag{2.22}$$

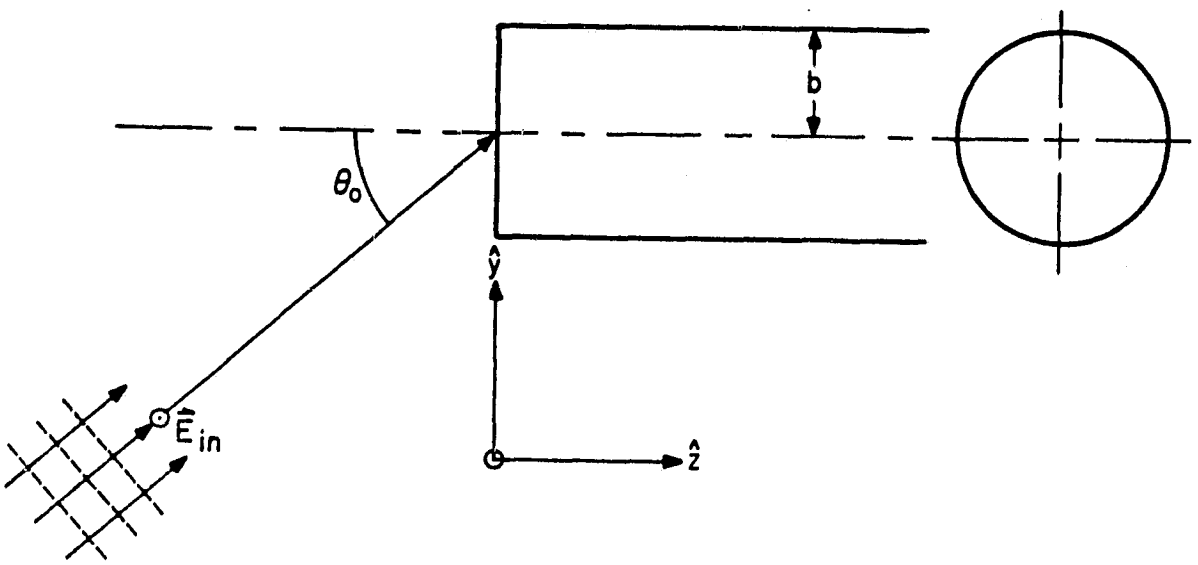

Figure 2. An open-ended cylindrical waveguide illuminated by an incident plane wave.

$$\vec{H}^{in} = \frac{E_o}{Z_o}\,\hat{y}\,\exp[-j(k_x x + k_z z)] \tag{2.23}$$

where θ_o is the incident angle, k_x and k_z are the components of the wave vector, E_o is a constant, and Z_o is the free-space impedance $\sqrt{\mu_o/\epsilon_o}$. Note that we choose the coordinate for the incident field in order to simplify the formulation. When the tangential E field at the opening of the waveguide is matched, the transmitted transverse fields at $z = 0$ are given by (Appendix 3)

$$\vec{E}_t(z = 0^+) = \sum_{m,n} C^H_{mn}\vec{U}^H_{mn} + \frac{\overline{k}_{zmn}}{k_o}\overline{C}^H_{mn}\vec{V}^H_{mn} \tag{2.24}$$

$$H_t(z = 0^+) = \frac{1}{Z_o}\sum_{m,n}\frac{k_{zmn}}{k_o}C^H_{mn}(\hat{z} \times \vec{U}^H_{mn}) + \overline{C}^H_{mn}(\hat{z} \times \vec{V}^H_{mn}) \tag{2.25}$$

where

$$\begin{bmatrix}\vec{U}^V_{mn}\\ \vec{U}^H_{mn}\end{bmatrix} = N_{mn}\left\{\hat{\rho}\,\frac{m}{\rho}\,J_m\left(\frac{\xi'_{mn}}{b}\,\rho\right)\begin{bmatrix}\sin m\phi\\ -\cos m\phi\end{bmatrix} + \hat{\phi}\,\frac{\xi'_{mn}}{b}\,J'_m\left(\frac{\xi'_{mn}}{b}\,\rho\right)\begin{bmatrix}\cos m\phi\\ \sin m\phi\end{bmatrix}\right\} \tag{2.26}$$

$$\begin{bmatrix}\vec{V}^V_{mn}\\ \vec{V}^H_{mn}\end{bmatrix} = \overline{N}_{mn}\left\{-\hat{\rho}\,\frac{\xi_{mn}}{b}\,J'_m\left(\frac{\xi_{mn}}{b}\,\rho\right)\begin{bmatrix}\sin m\phi\\ \cos m\phi\end{bmatrix} + \hat{\phi}\,\frac{m}{\rho}\,J_m\left(\frac{\xi_{mn}}{b}\,\rho\right)\begin{bmatrix}-\cos m\phi\\ \sin m\phi\end{bmatrix}\right\} \tag{2.27}$$

$$C^H_{mn} = -\frac{E_o}{Z_o}\cos\theta_o\,N_{mn}\,\frac{2\pi m}{k_x}\,(-j)^{m-1}\,J_m(\xi'_{mn})\,J_m(k_x b) \tag{2.28}$$

$$\overline{C}_{mn} = -\frac{E_o}{Z_o} \cos\theta_o \, \overline{N}_{mn} \frac{2\pi\xi_{mn}(-j)^{m-1}}{k_x^2 - \left(\frac{\xi_{mn}}{b}\right)^2} \, k_x J_m'(\xi_{mn}) \, J_m(k_x b) \tag{2.29}$$

Here k_o is the free-space wave number $\omega\sqrt{\mu_o \varepsilon_o}$, and $\vec{U}$ and $\vec{V}$ indicate the normalized TE and TM fields, respectively. The superscripts V and H indicate the vertical and horizontal polarizations, respectively. The symbols with an over bar indicate TM modes and these without an over bar, TE modes. N_{mn} and $\overline{N}_{mn}$ are the normalization constants (Appendix 3).

When we match the tangential magnetic field, the expressions for the transmitted transverse fields at $z = 0$ are similar to the above expressions except for the $\cos\theta_o$ terms in Eqs. (2.28) and (2.29) and the factor of k_{zmn}/k_o (Appendix 3). In this report, we use the electric-field matching.

In order to characterize the power attenuation of the transmitted wave, we approximate the modal fields in the lossy waveguide by the modal fields in the perfect waveguide with the exception of the z-dependence of the propagation constant, which characterizes the wave attenuation. Then the power propagating within the lossy waveguide from a normally incident plane wave is approximately given by (Appendix 3)

$$\frac{P(z)}{P_o} \approx 2\sum_n \frac{(\beta_{1n}/k_o)\exp[-2\alpha_{1n}z]}{(\xi_{1n})^2 - 1} \tag{2.30}$$

where

$$k_{z1n} = \beta_{1n} - j\alpha_{1n} \tag{2.31}$$

Here P_o is the power incident on the area of the opening of the waveguide and β_{1n} and α_{1n} are the real and imaginary parts of the propagation constant, respectively.

We note in Eq. (2.30) that the higher mode usually carries less power because the higher mode has a smaller β_{1n} but a larger ξ'_{1n}.

3. NUMERICAL RESULTS

Numerical results are given for the dominant TE_{11} and TM_{11} modes for the purpose of comparison. The cutoff frequencies of lower-order modes in terms of the cutoff frequency of the dominant mode are shown in Figure 3. The mode patterns of 30 lowest modes are shown in Figures 4 and 5.

3.1. Mode Attenuation and Dispersion

3.1.1. Frequency dependence

Figures 6 and 7 show the real and imaginary parts of the propagation constants of the TE_{11} and TM_{11} modes as a function of frequency in a waveguide coated with a thin dielectric material. In Figure 6, the exact numerical solutions for the attenuation constants are compared with the results obtained from the perturbation theory (Section 2.1.1). We can see that the perturbation theory is valid only at the low-frequency region even though the thickness of the dielectric layer is small. At the high-frequency region, the TE_{11} mode shows much higher attenuation than the TM_{11} mode. This is due to the fact that the TE_{11} modal field moves closer to the surface of the waveguide than the TM_{11} mode as frequency increases. These features are shown in Figures 8 and 9, where the magnitudes of the angular and radial electric fields are plotted as a function of radial distance. Note that the fields of both TE_{11} and TM_{11} modes at the low frequency (3 GHz) are similar to those for the unperturbed case, but the modal fields of the TE_{11} mode (Figure 8) are closer to the surface than those of the TM_{11} mode (Figure 9) at the high frequency (7 GHz). On the other hand, the real part of the propagation constant is not much different from that for the unperturbed case (Figure 6).

3.1.2. Dielectric constant dependence - thin layer

Figures 10 and 11 show the attenuation constants as a function of the complex dielectric constant ε_r of the lossy dielectric material. We observe two

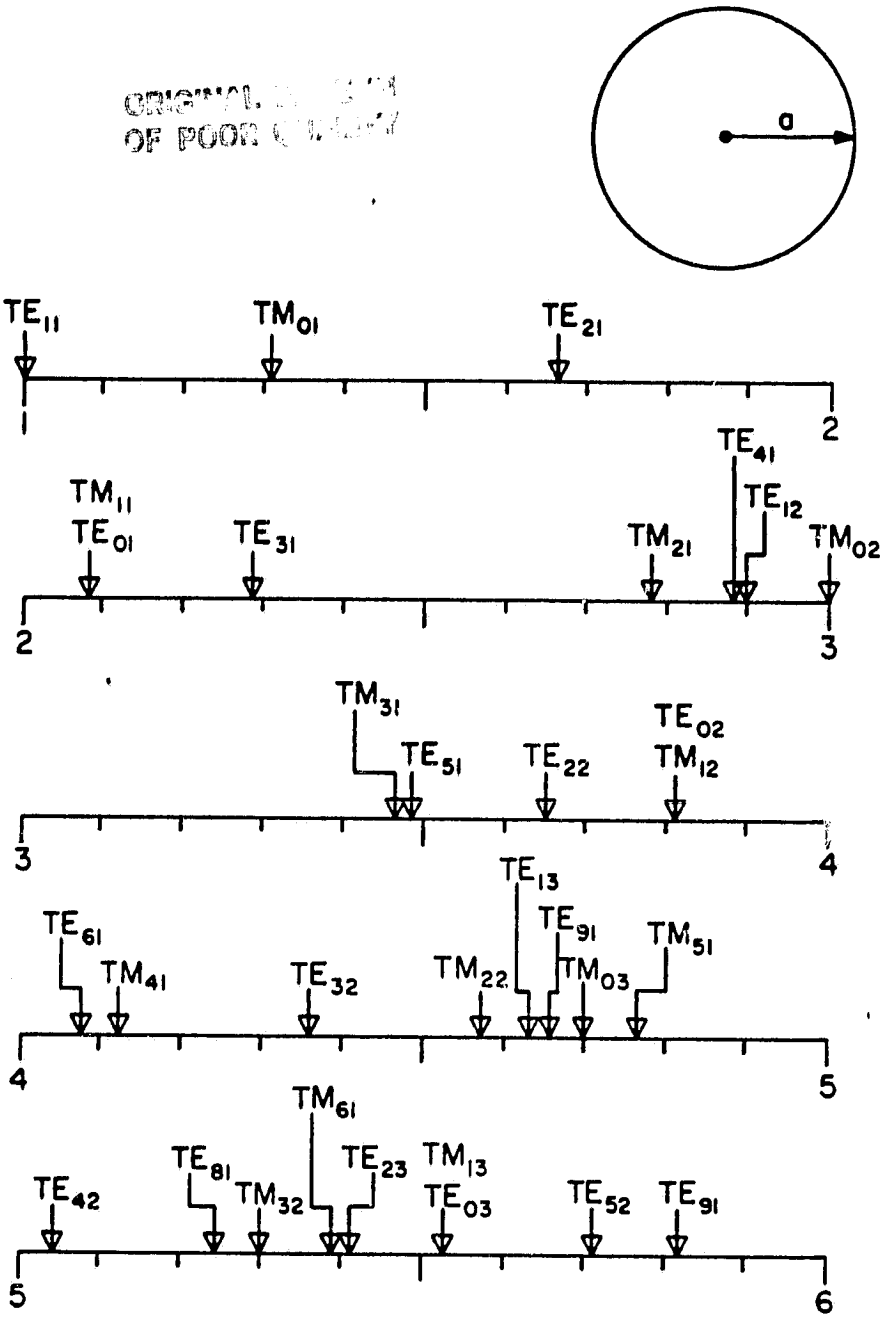

Figure 3. The ratios of cutoff frequencies of lower-order modes to the cutoff frequency of the dominant mode (TE_{11}) in a circular waveguide.

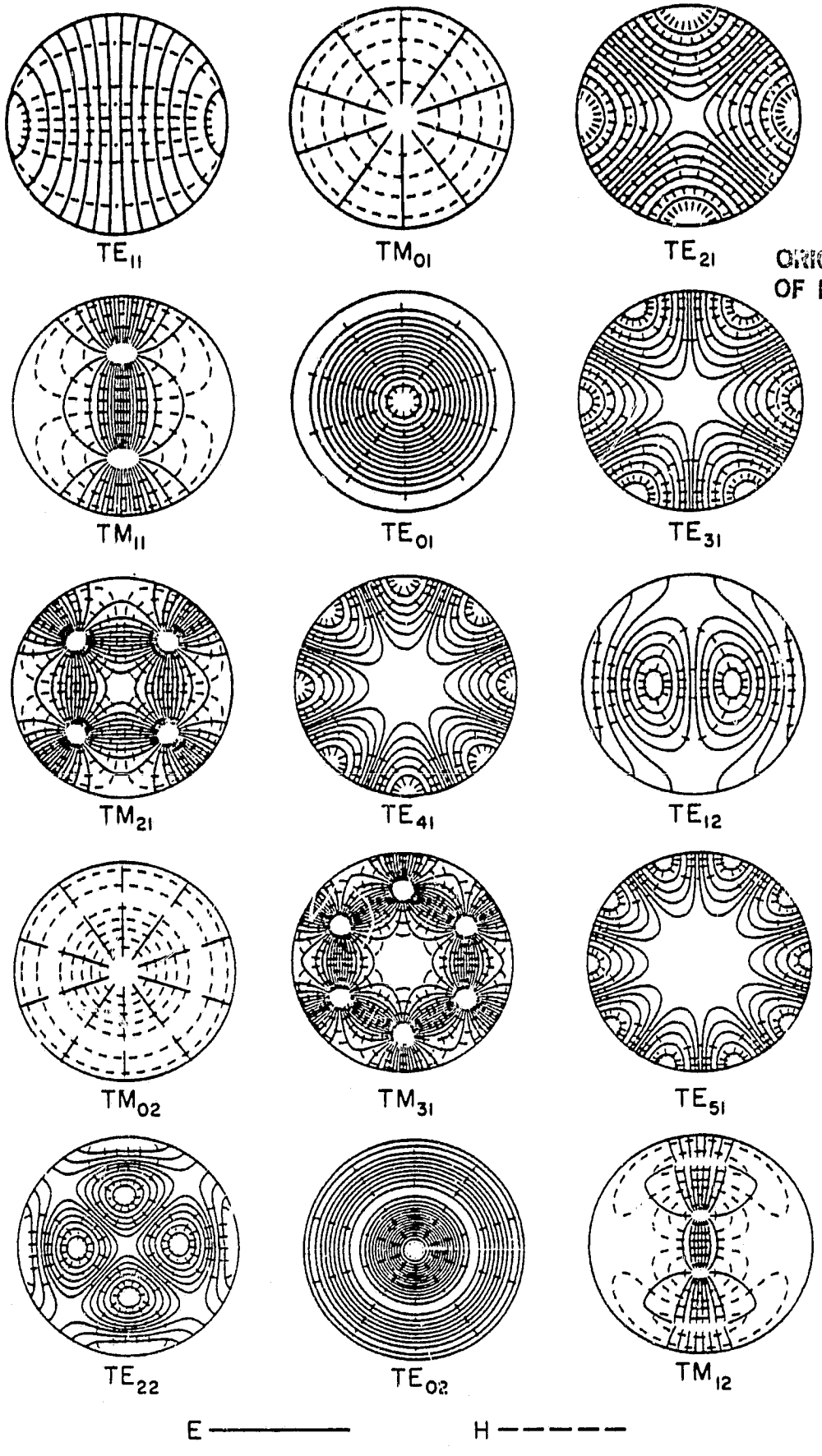

Figure 4. Mode patterns of first 15 lowest modes in a circular waveguide.

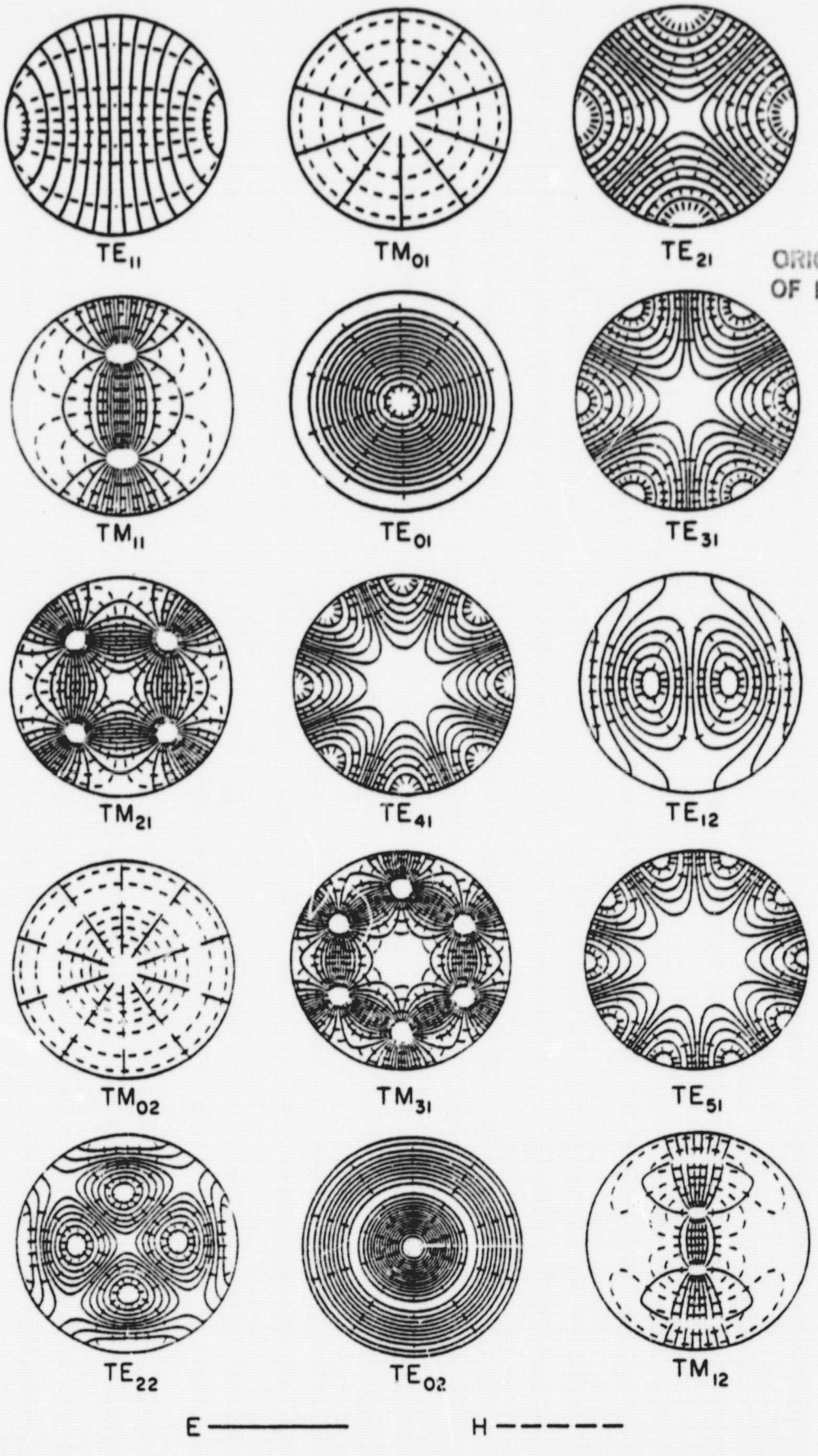

Figure 4. Mode patterns of first 15 lowest modes in a circular waveguide.

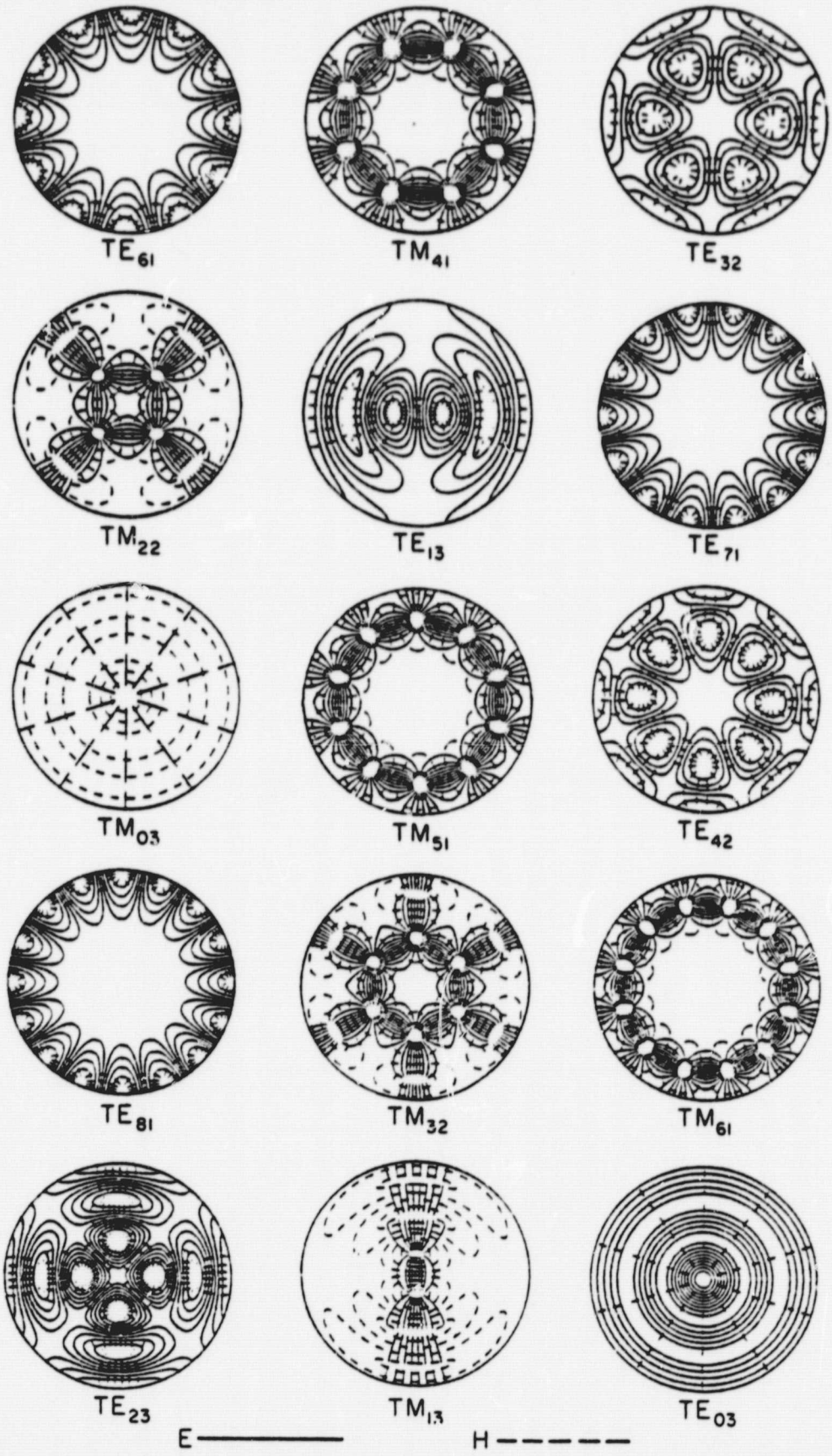

Figure 5. Mode pattern of second 15 lowest modes in a circular waveguide.

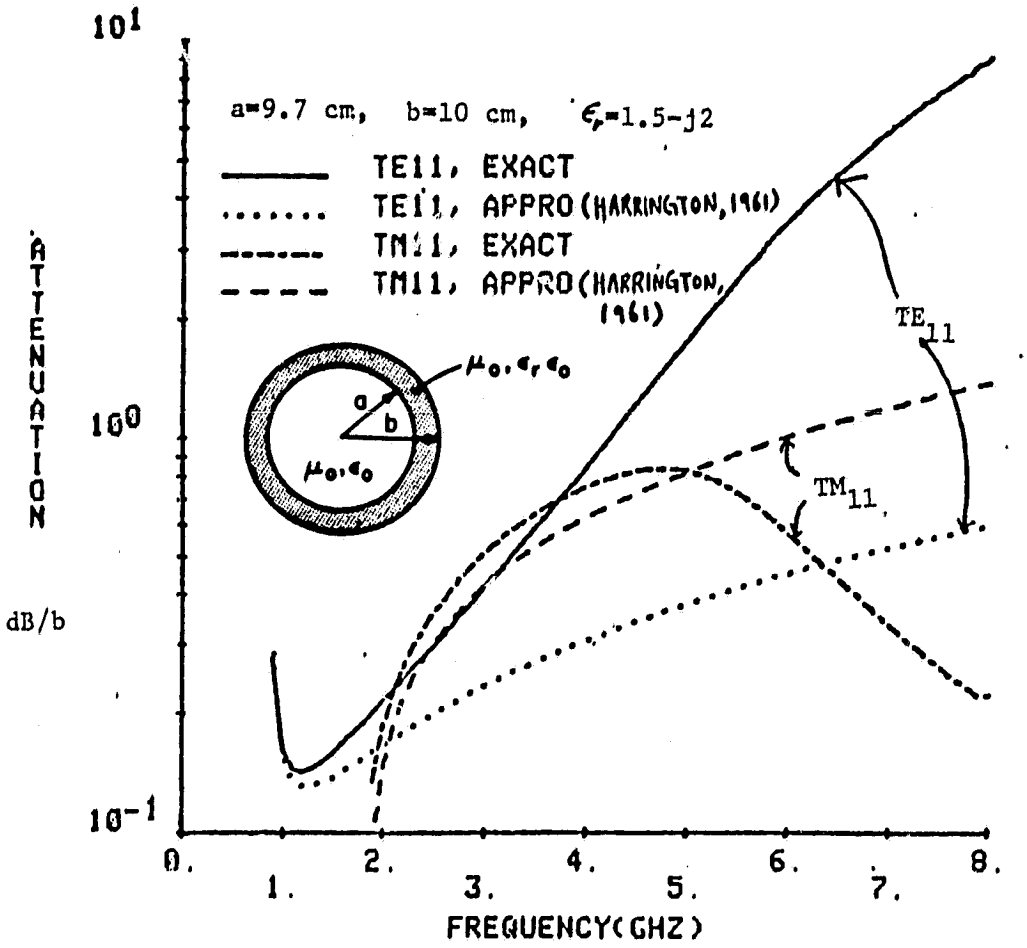

Figure 6. Attenuation constant as a function of the frequency.

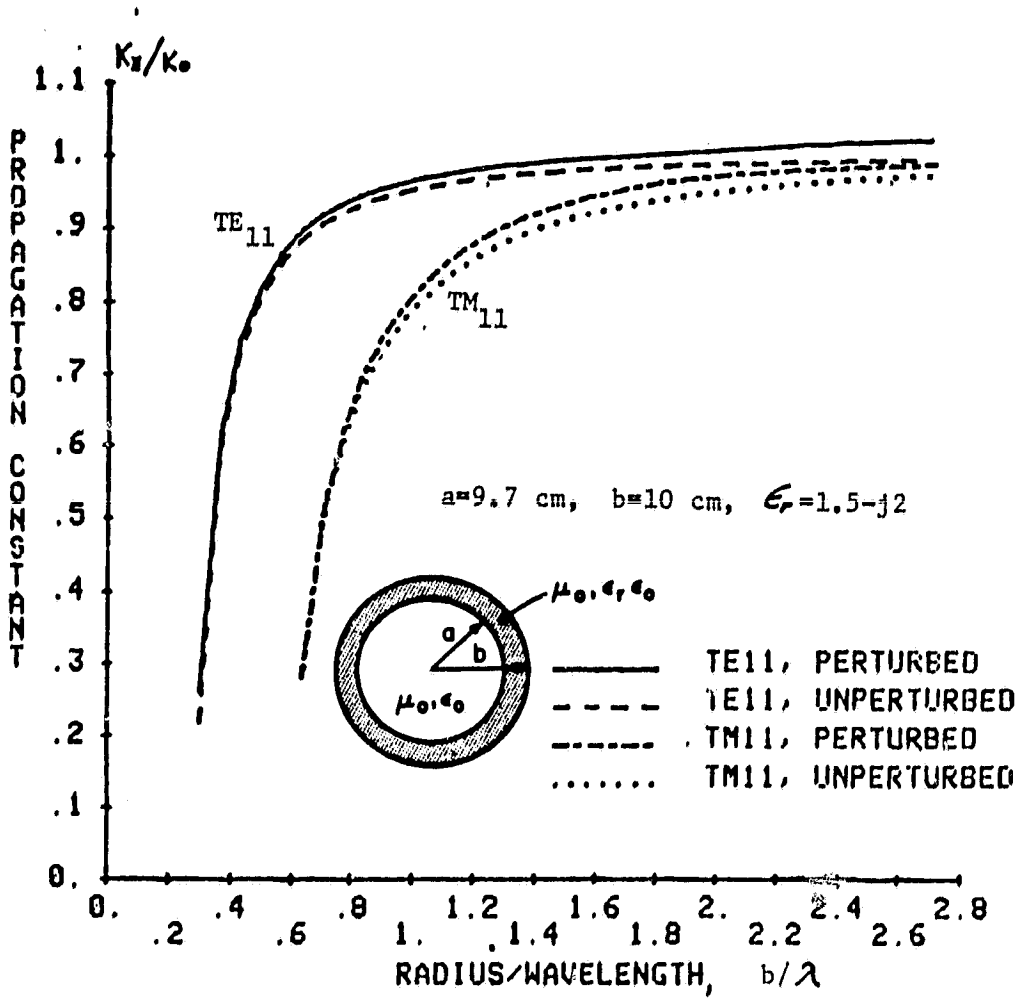

Figure 7. Real part of the propagation constant.

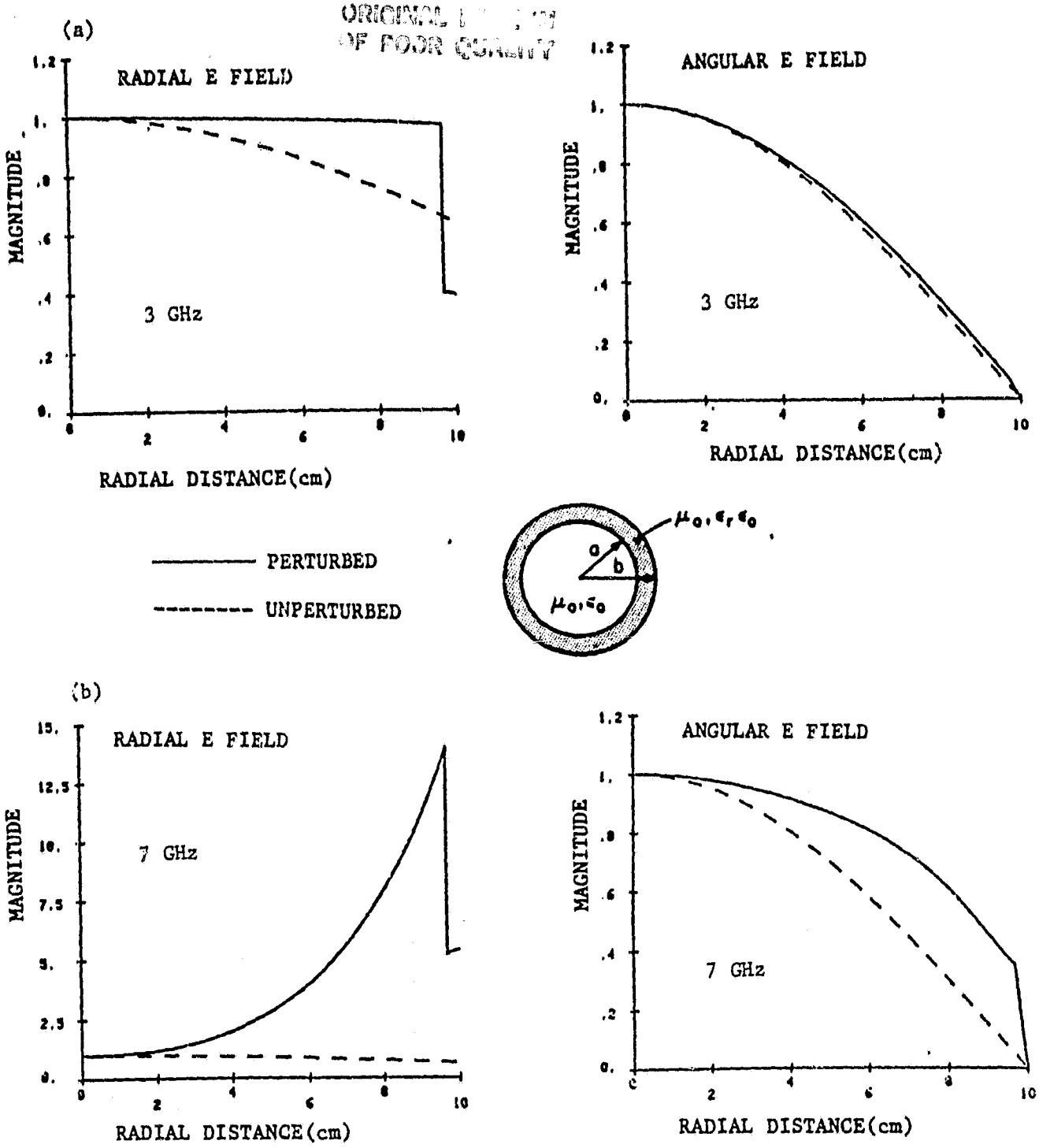

Figure 8. Radial and angular components of the electric field of the TE_{11} mode relative to the fields at $\rho = 0$: $\varepsilon_2 = 1.5 - j2$, a = 9.7 cm, b = 10 cm, a) f = 3 GHz, b) f = 7 GHz.

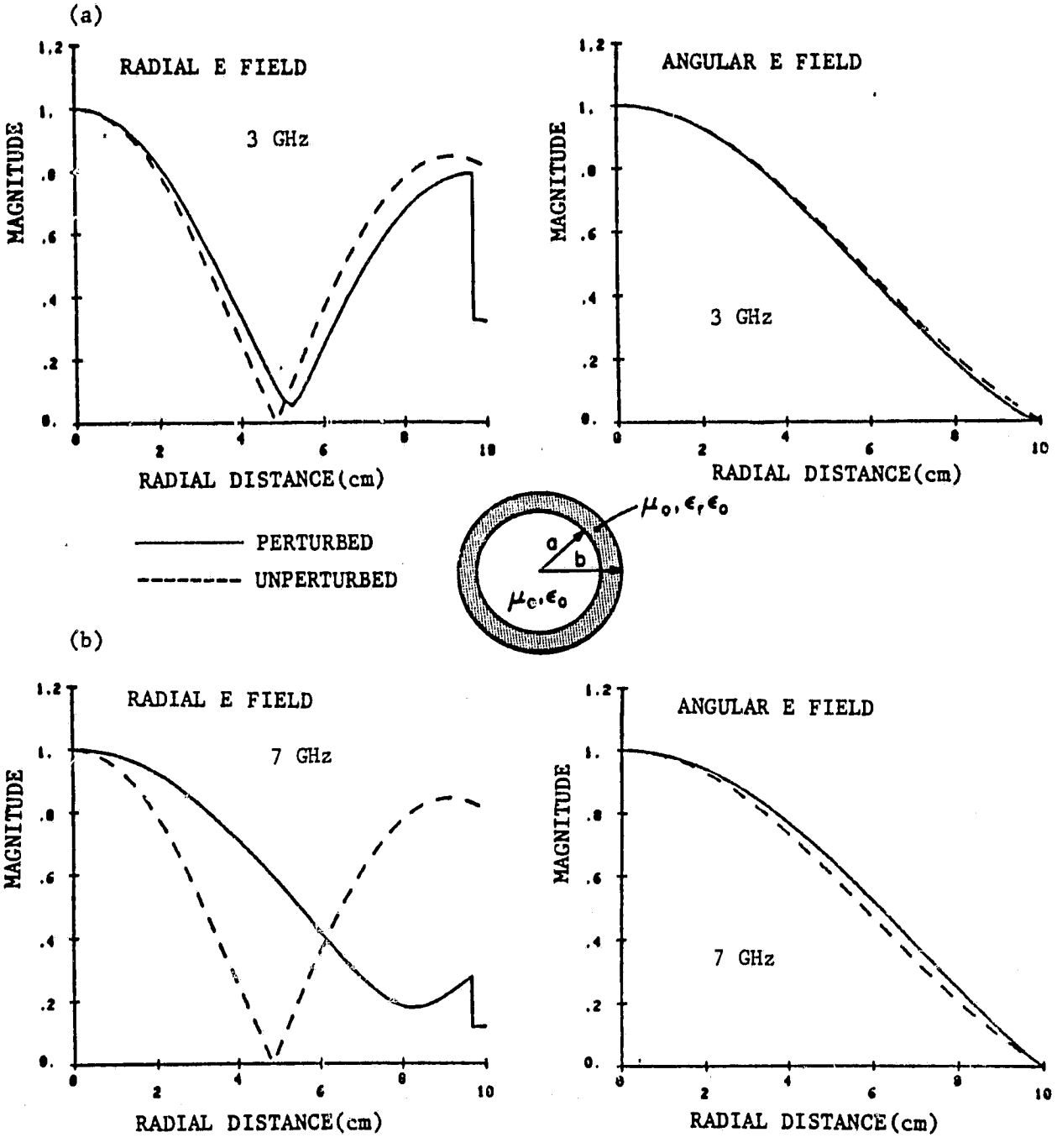

Figure 9. Radial and angular components of the electric field of the TM_{11} model relative to the fields at $\rho = 0$: $\varepsilon_2 = 1.5 - j2$, a = 9.7 cm, b = 10 cm, a) f = 3 GHz, b) f = 7 GHz.

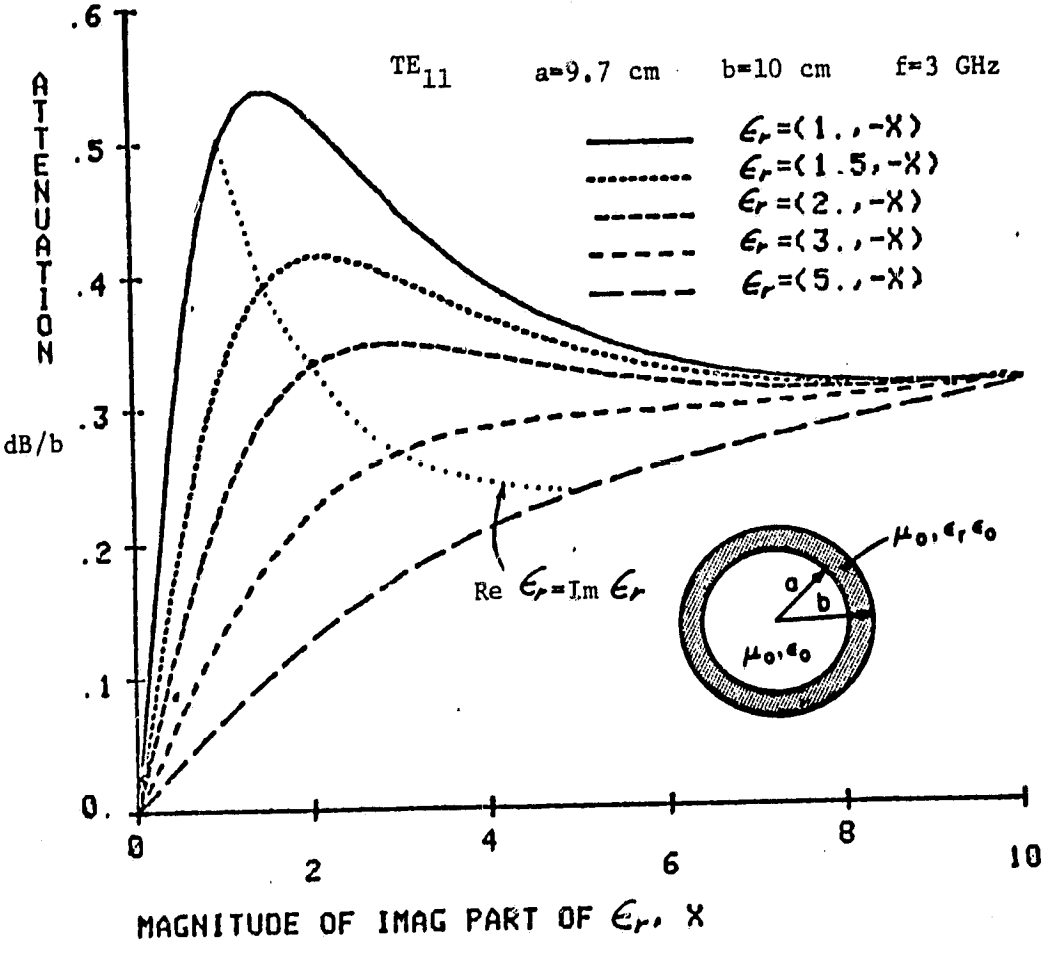

Figure 10. Attenuation constant as a function of $\epsilon_r^I(TE_{11})$.

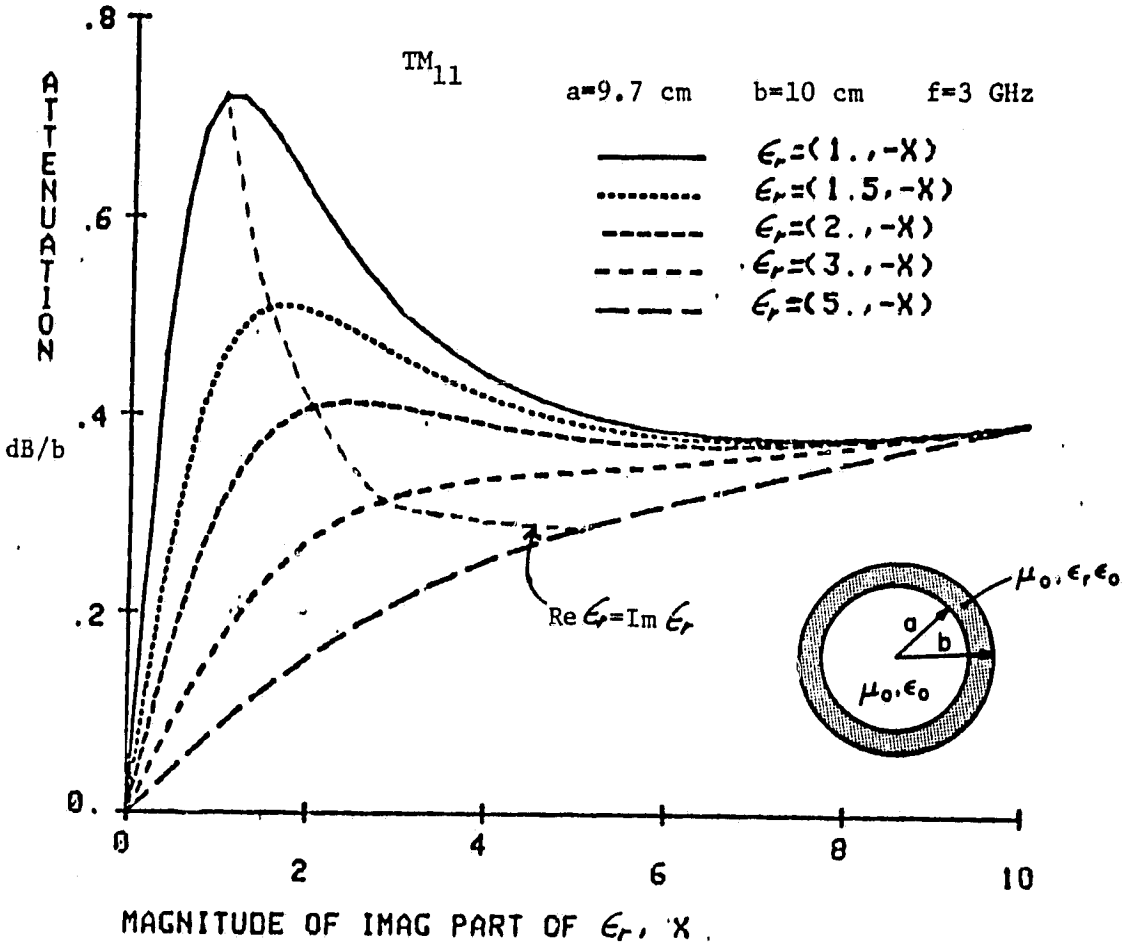

Figure 11. Attenuation constant as a function of $\varepsilon_r^I(TM_{11})$.

interesting features in these graphs. First, there is a clear "resonance" effect of the imaginary part ε_r^I of ε_r on the attenuation constant when the real part of ε_r^R of ε_r is small ($\lesssim 1.5$). Second, a smaller ε_r^R gives a larger attenuation constant except for that with a "dielectric resonance." Since the ε_r^R of the practical materials are usually larger than 1.5, we need to choose the lossy dielectric material with a large loss tangent (small ε_r^R but large ε_r^I) for a large power attenuation in the waveguide.

Note that the general dependence of the attenuation constant on the dielectric constant for both TE_{11} and TM_{11} are very similar, and these properties may not be limited to those two particular modes. To understand these results, consider the following. The attenuation constant is proportional to the power dissipation within the lossy dielectric layer. The power dissipation per unit length P_d is related by

$$P_d = \frac{\omega}{2} \int_{\varepsilon\text{-layer}} |\varepsilon_r^I| |\vec{E}|^2 \, dS$$

where the integration is over the dielectric region. Then the attenuation constant is given by

$$\text{Im } k_z = \frac{\omega \int_{\varepsilon\text{-layer}} |\varepsilon_r^I| |\vec{E}|^2 \, dS}{2 \int \vec{E} \times \vec{H}^* \cdot \hat{z} \, dS} \tag{3.1}$$

where the integration in the denominator is over the cross-sectional area. Hence for a large attenuation constant, we need a large ε_r^I and large field concentration within the dielectric layer. These properties can be illustrated from the field distributions within the waveguide (Figures 12 and 13). The tangential electric fields are usually small in the dielectric region with a thin dielectric layer because the tangential electric fields vanish on a

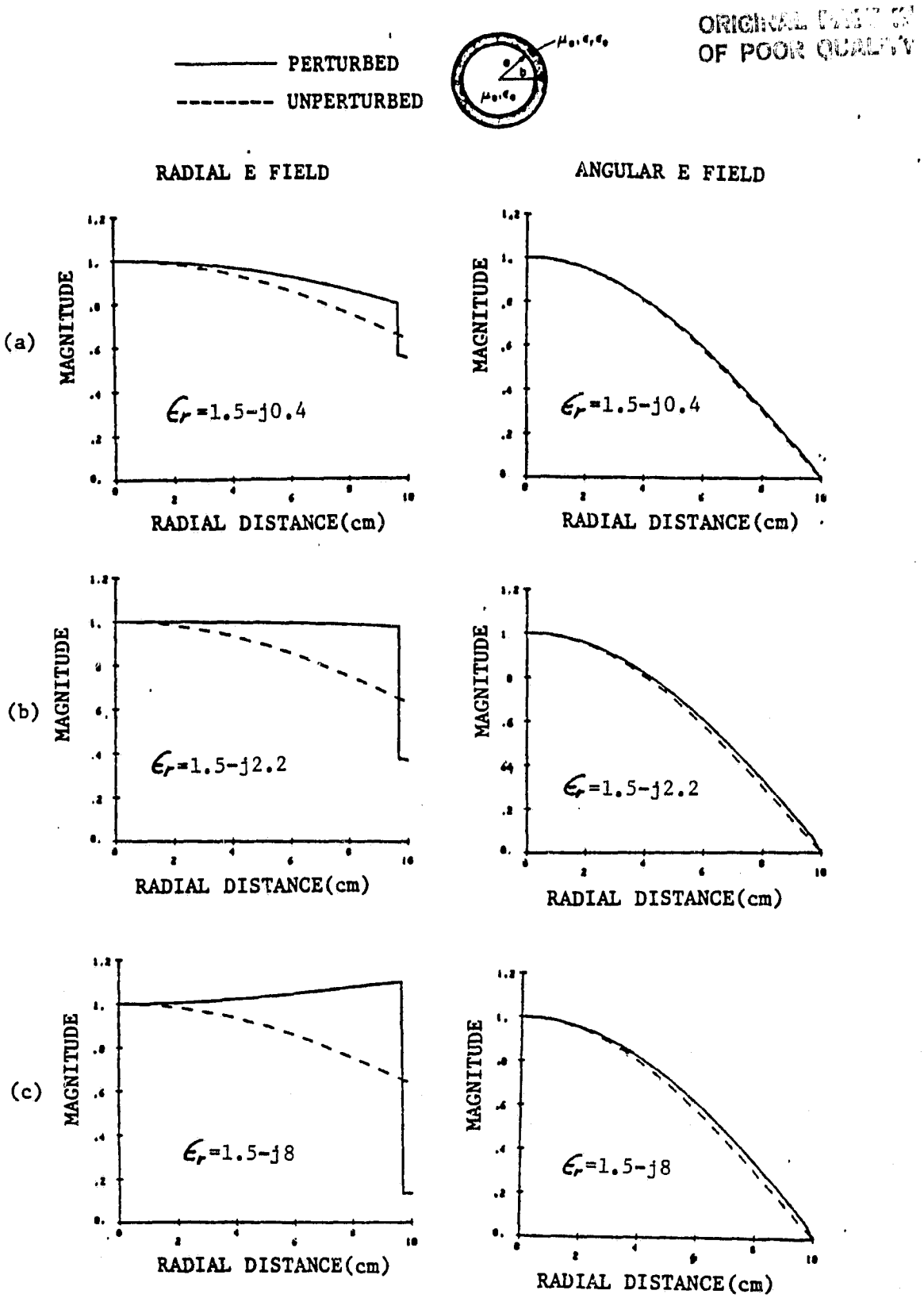

Figure 12. Radial and angular components of the electric field of the TE_{11} mode relative to the fields at $\rho = 0$: f = 3 GHz, a) $\epsilon_r = 1.5 - j0.4$, b) $\epsilon_r = 1.5 - j2.2$, c) $\epsilon_r = 1.5 - j8$.

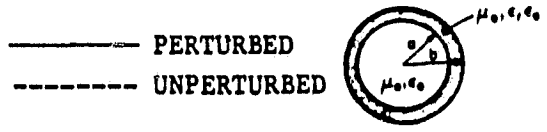

RADIAL E FIELD

ANGULAR E FIELD

(a)

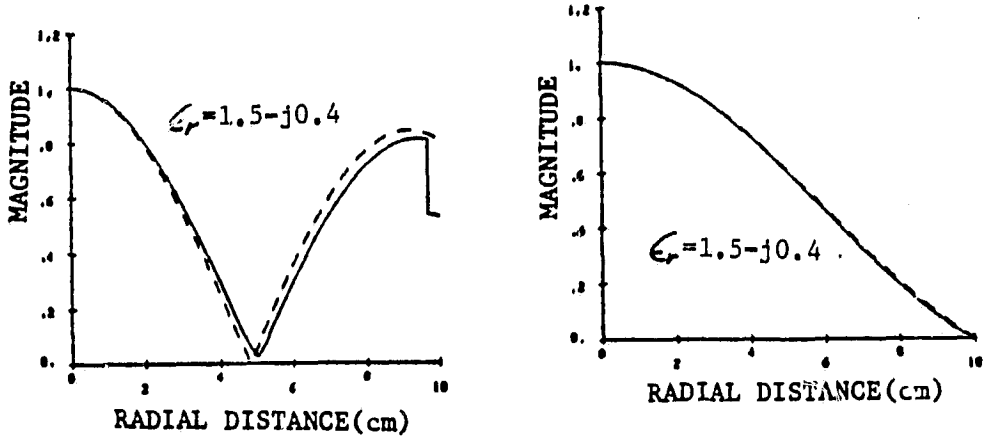

(b)

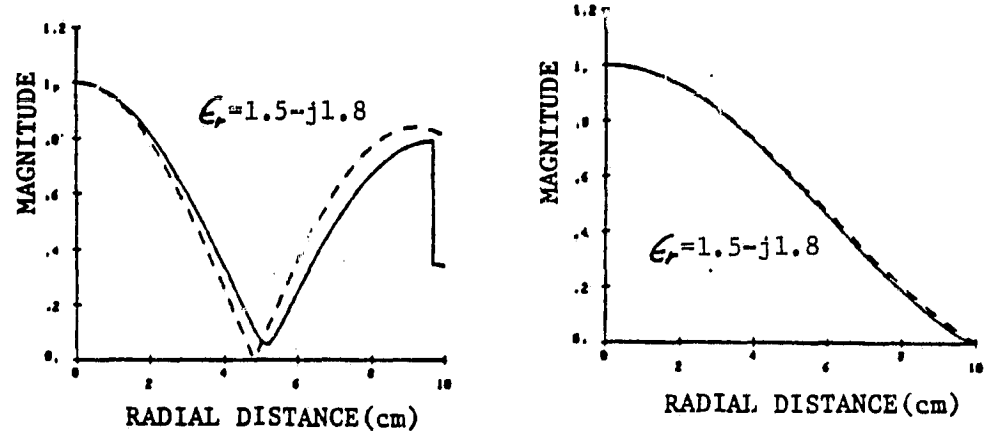

(c)

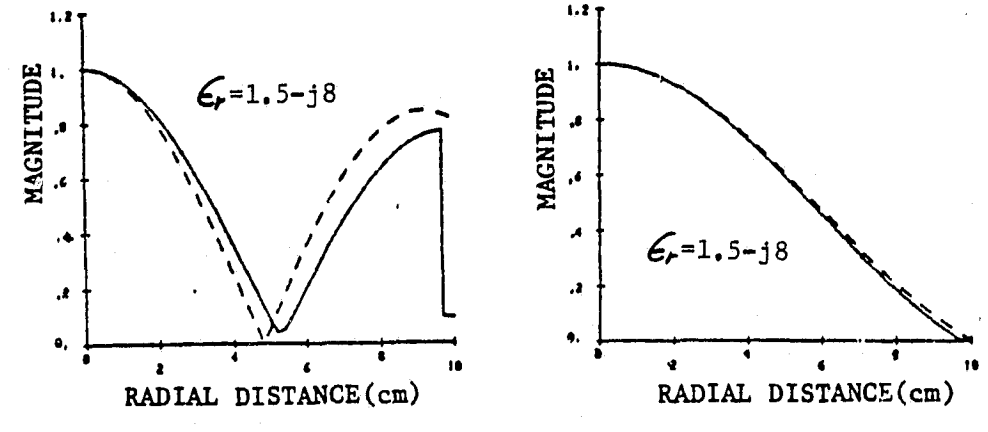

Figure 13. Radial and angular components of the electric field of the TM_{11} mode relative to the fields at $\rho = 0$: f = 3 GHz, a) $\varepsilon_r = 1.5 - j0.4$, b) $\varepsilon_r = 1.5 - j1.8$ c) $\varepsilon_r = 1.5-j8$.

perfectly conducting surface. These features are shown in Figures 12 and 13 as well as the field expressions in Section 2.1.2. The ratios of the tangential fields to the radial fields are approximately given by

$$\frac{E_\phi}{E_\rho} \simeq \tau/b \tag{3.2}$$

$$\frac{E_z}{E_\rho} \simeq \frac{k_{\rho 2}^2 \tau}{k_z} \qquad \text{for TM(EH)} \tag{3.3}$$

$$\frac{E_\phi}{E_\rho} \simeq k_{\rho 2} b \frac{\tau}{b} \qquad \text{for TE(HE), } m \neq 0 \tag{3.4}$$

Since $k_{\rho 2}\tau$ and τ/b are small for a thin dielectric layer, these ratios are usually small. Thus E_ρ is responsible for most of the power loss. Since E_ρ at the dielectric region is inversely proportional to $|\varepsilon_r|$ (see eq. (A1.7)), increasing ε_r^I decreases the electric-field strength within the dielectric layer (Figures 12 and 13). Since the power loss is also proportional to $|\varepsilon_r^I|$, there may exist an optimum value of ε_r^I for a maximum power loss and a maximum attenuation constant (Figures 12b and 13b).

We expect the attenuation constant to become vanishingly small as ε_r^I becomes very large, because the dielectric layer becomes a perfect conductor in this limit. These features are shown in Figures 14 and 15, where the attenuation constants in the asymptotic limit of ε_r^I are plotted as a function of ε_r^I. Note that the attenuation constants decay rather slowly as ε_r^I becomes very large.

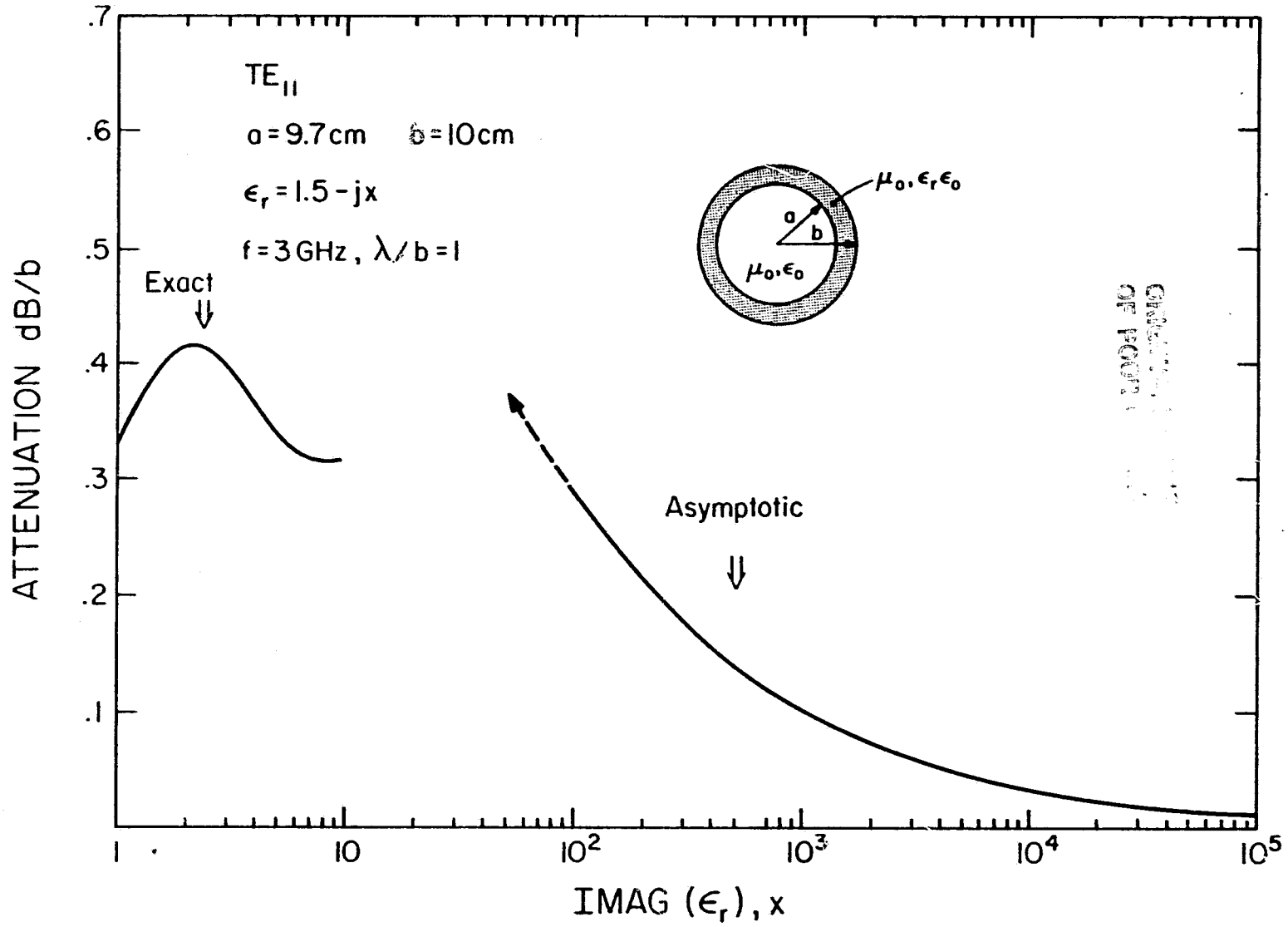

Figure 14. Asymptotic behavior of the propagation constant of TE_{11} with the variation of the imaginary part of ϵ_r ($\epsilon_r = 1.5 - jx$).

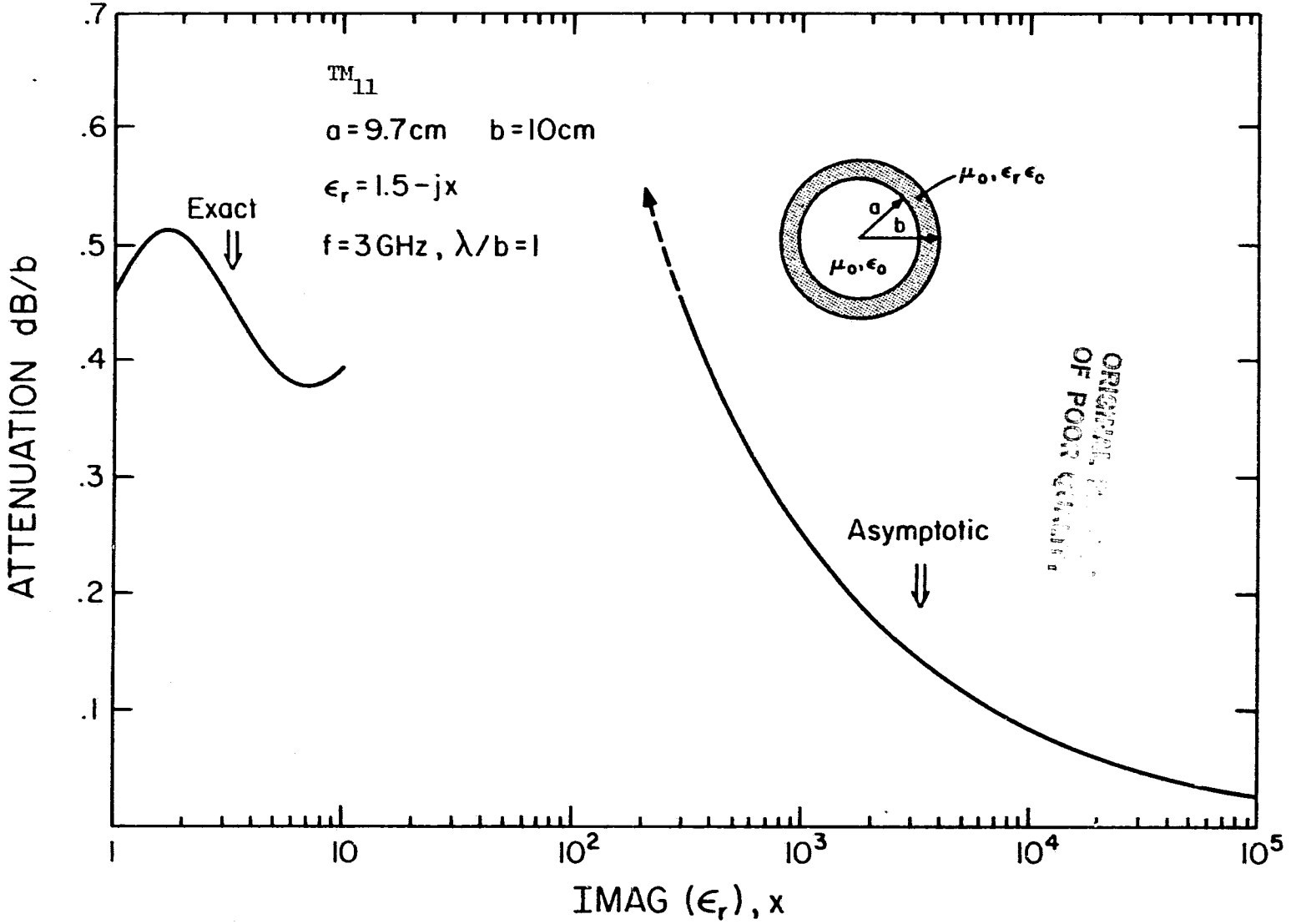

Figure 15. Asymptotic behavior of the propagation constant of TM_{11} with the variation of the imaginary part of ϵ_r ($\epsilon_r = 1.5 - jx$).

3.1.3. Dielectric-thickness dependence

When the dielectric layer is thick, the behavior of the propagation constant is different from that in the case of the thin dielectric layer. These features are shown in Figures 16, 17, 18, and 19. We observe a few interesting points in these figures.

First, there may exist a "spatial"-resonance effect as the layer thickness increases. That is, there may exist an optimum layer thickness for a large attenuation constant. As shown in Figure 20, the optimum thickness results when the thickness of the dielectric layer is about 1/4 of the wavelength within the dielectric layer. This is contrary to the common belief that the thicker the lossy layer is, the larger the attenuation constant becomes. It is interesting to note that when the resonance is weak (e.g., TE with a small ε_r^I), the field is similar to the field of a surface mode confined to the dielectric region near the surface. This feature is shown in Figure 21a, where the ratios of the magnitudes of the electric fields to those at the center of the waveguide are plotted as a function of the radial distance.

Second, when we keep the ratio of ε_r^I to ε_r^R (i.e., the loss tangent) constant, the basic dependence of the attenuation constant on the dielectric-layer thickness remains similar. Generally, a thicker layer attenuates the TE mode more significantly than the TM mode.

Third, as ε_r^I increases, the attenuation constant of the TM_{11} mode increases, but the attenuation constant of the TE_{11} mode decreases. This can be understood from the field distributions as shown in Figures 21 and 22. Note that when ε_r^I increases, the electric field of the TE_{11} mode at the dielectric region decreases significantly while the electric field of the TM_{11} mode remains relatively unchanged. Since the attenuation constant is also proportional

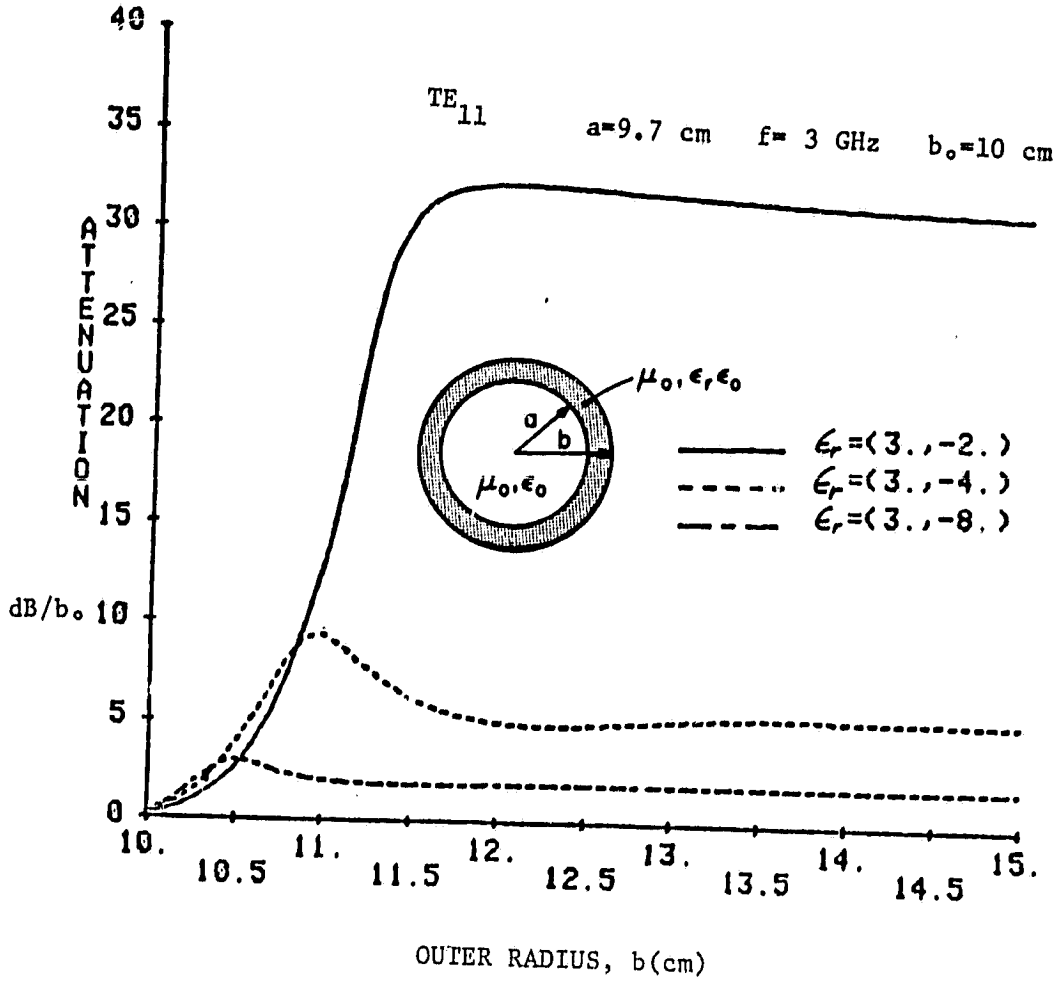

Figure 16. Attenuation constant with the variation of $b(TE_{11}, \varepsilon_r^R = 3)$.

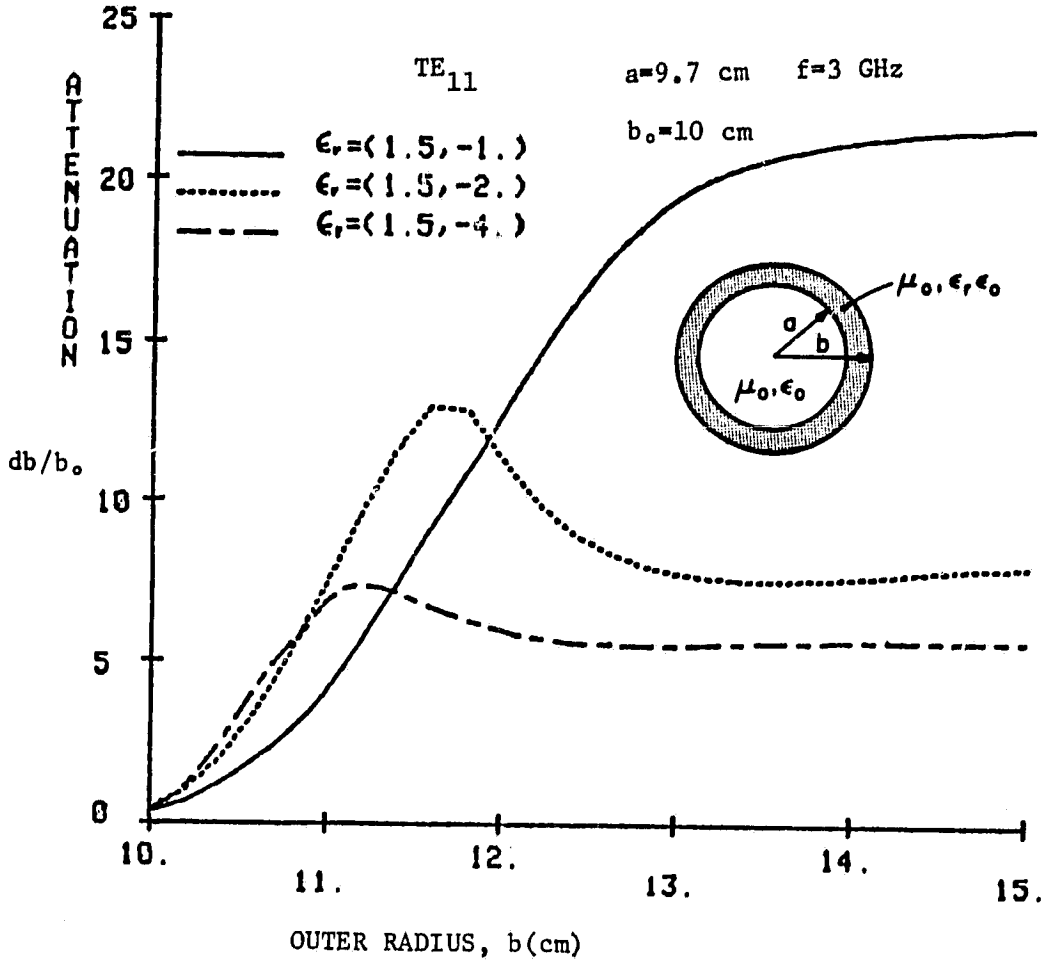

Figure 17. Attenuation constant with the variation of $b(TE_{11}, \epsilon_r^R = 1.5)$.

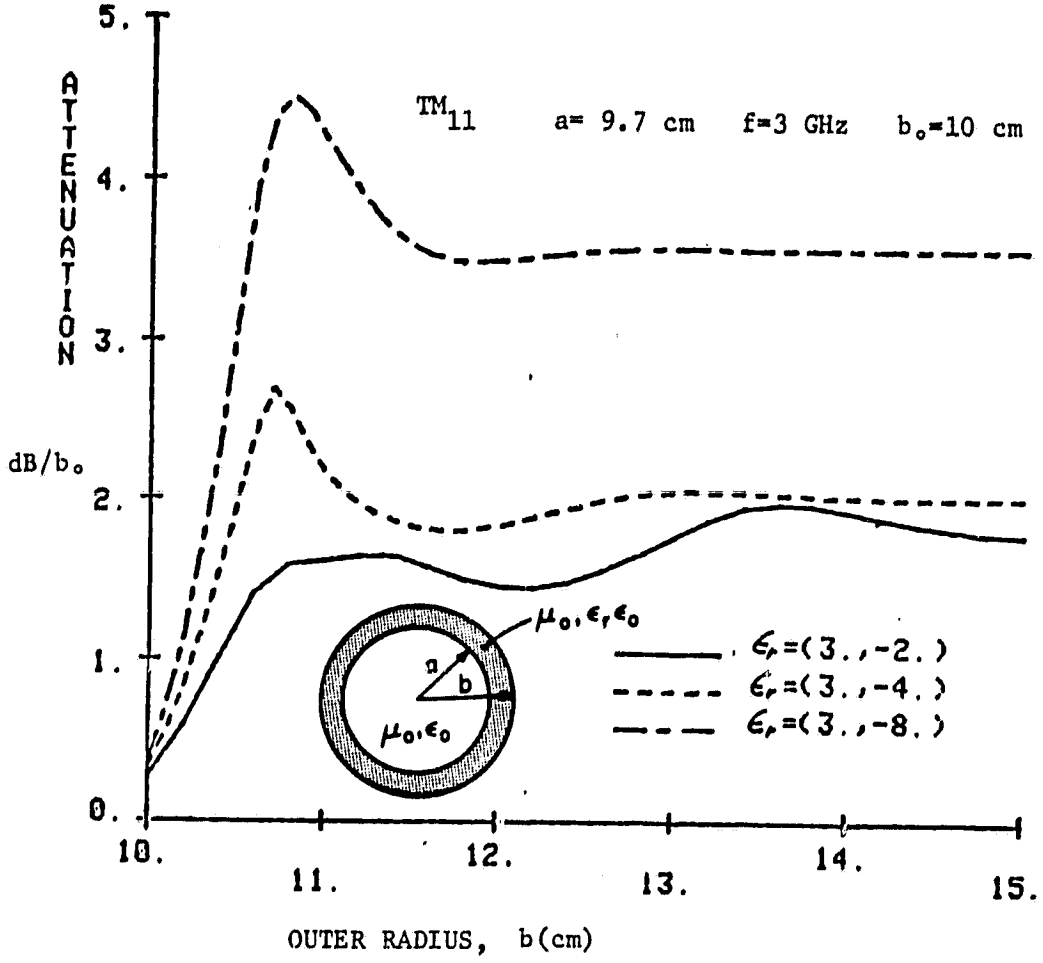

Figure 18. Attenuation constant with the variation of b (TM_{11}, $\epsilon_T^R = 3$).

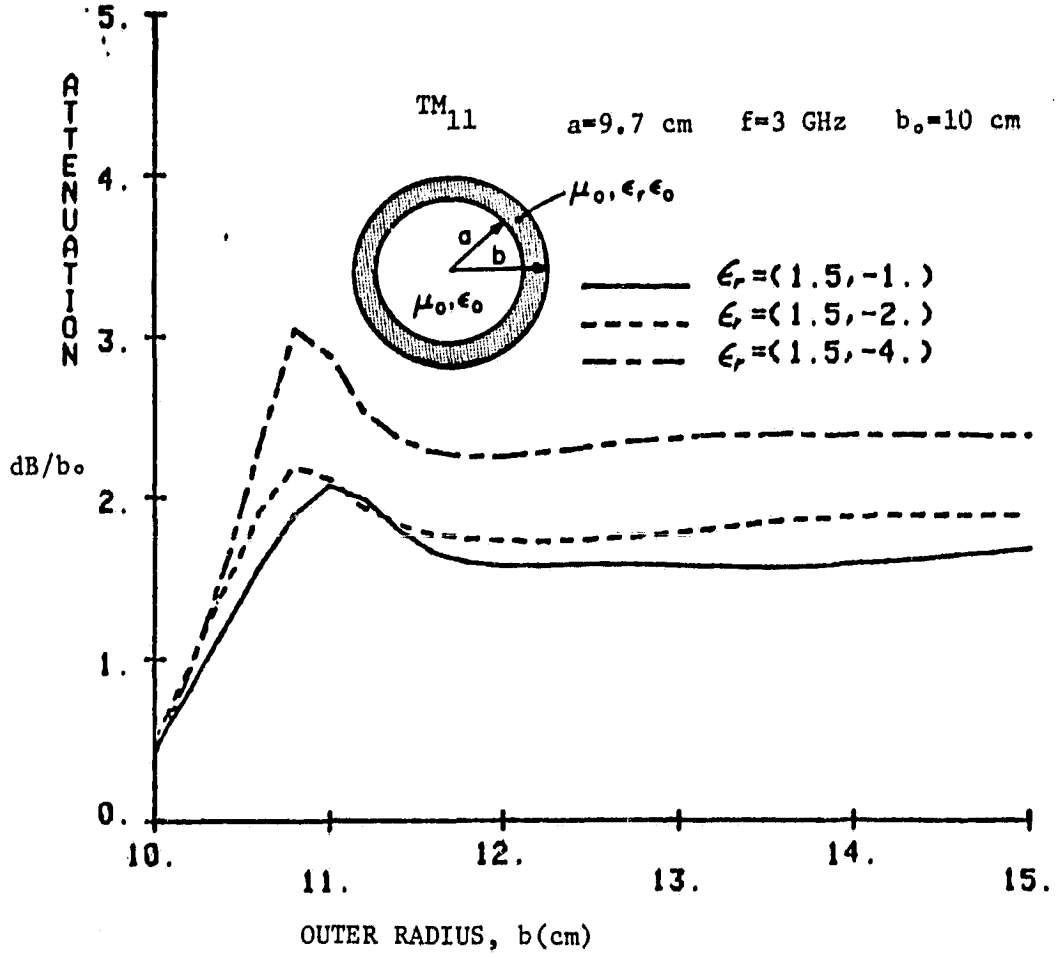

Figure 19. Attenuation constant with the variation of b (TM_{11}, $\epsilon_r^R = 1.5$).

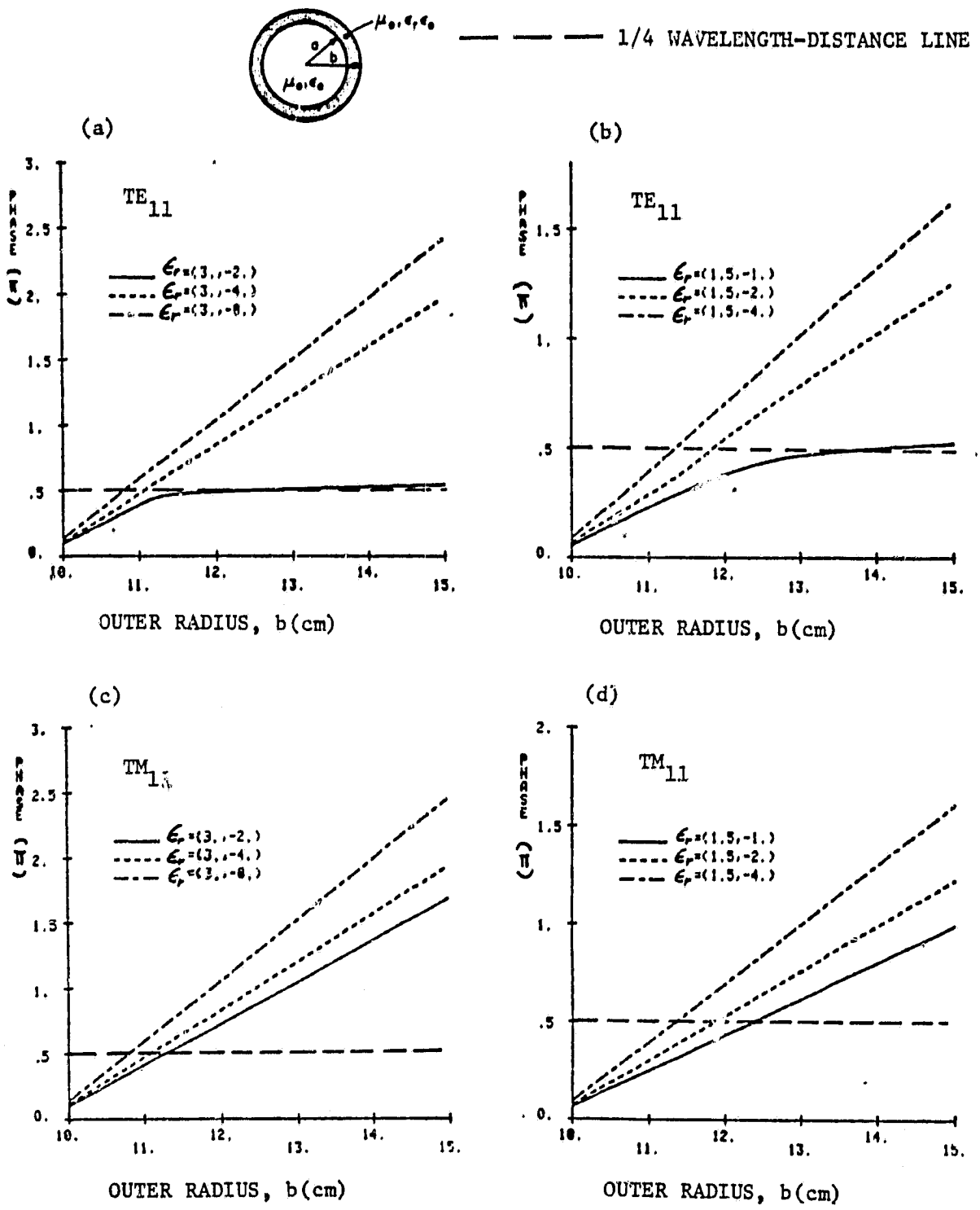

Figure 20. The phase distances of the normal modes in wavelength in the radial direction within the dielectric layer (phase = Real($k_{\rho 2}$)(b-a)/π) with the variation of b(a = 9.7 cm, f = 3 GHz): a) TE_{11}, ε_r^R = 3 (Figure 16), b) TE_{11}, ε_r^R = 1.5 (Figure 17), c) TM_{11}, ε_r^R = 3 (Figure 18), d) TM_{11}, ε_r^R = 1.5 Figure (19).

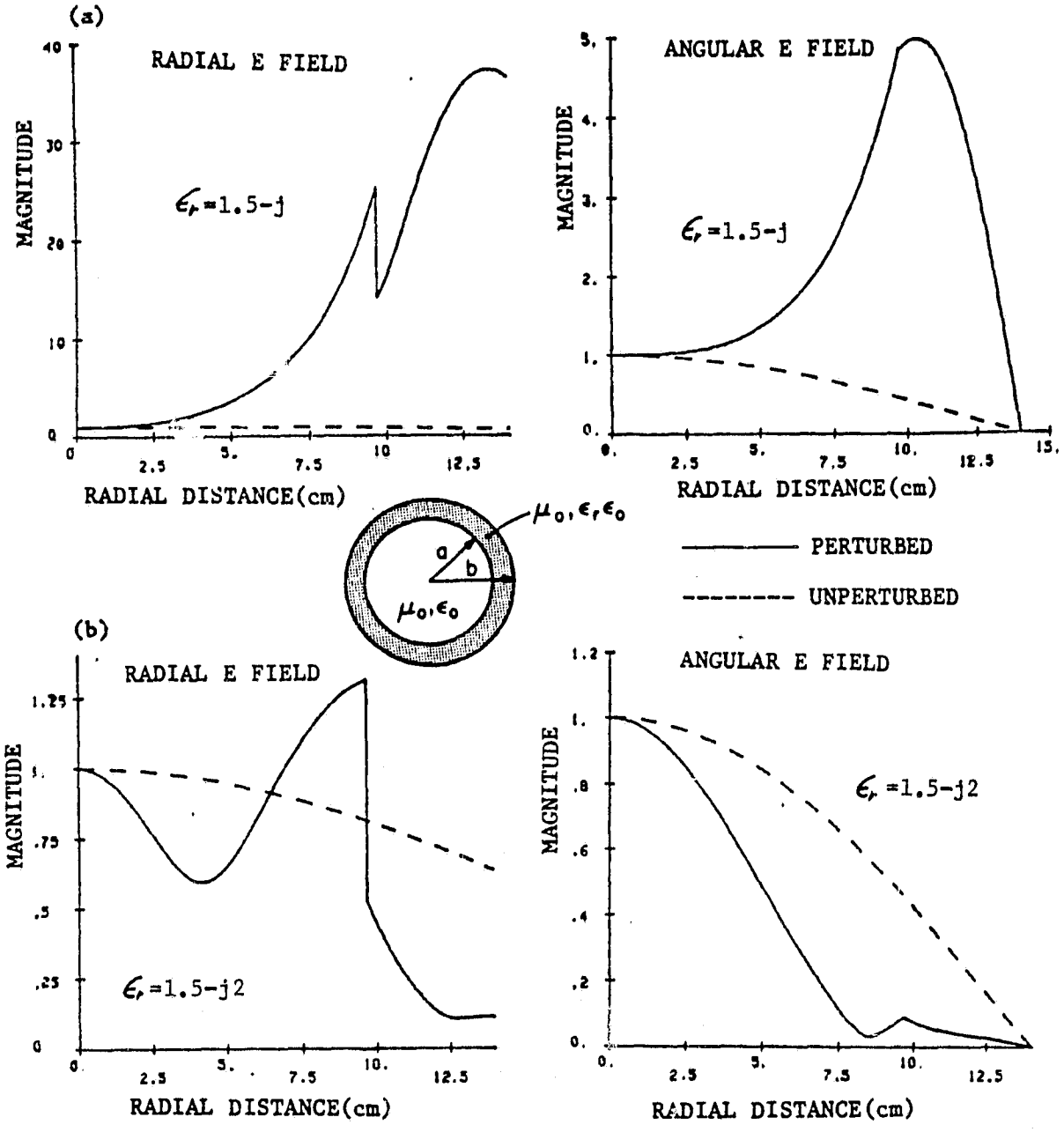

Figure 21. Radial and angular components of the electric field relative to the fields at $\rho = 0$ (thicker layer case): a = 9.7 cm, b = 14 cm, a) TE_{11}, $\epsilon_r = 1.5 - j$, b) TE_{11}, $\epsilon_r = 1.5 - j2$.

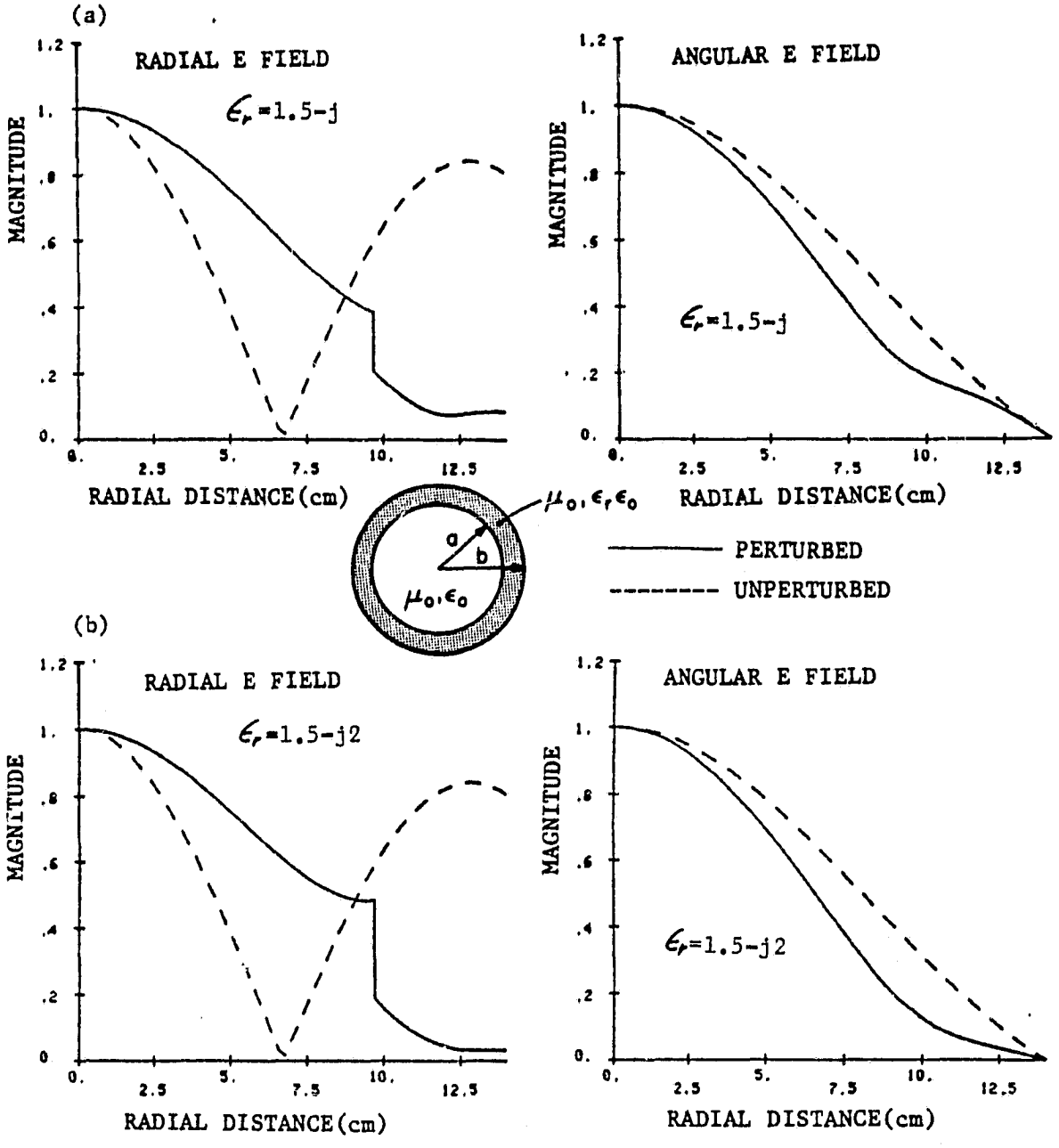

Figure 22. Radial and angular components of the electric field relative to the fields at $\rho = 0$ (thicker layer case): a = 9.7 cm, b = 14 cm, a) TM_{11}, $\epsilon_r = 1.5 - j$, b) TM_{11}, $\epsilon_r = 1.5 - j2$.

to ε_r^I (Equation (3.1)), the attenuation constant of the TM_{11} mode increases while the attenuation constant of the TE_{11} mode decreases as the ε_r^I of the lossy dielectric increases.

3.2. Wave Attenuation in the Lossy Waveguide from a Normally Incident Plane Wave

As shown in Section 3.1.2, the lossy dielectric with a large loss tangent is a good choice for the coating material for a large wave attenuation within the waveguide. Plastics are in this category [8]; three materials are chosen for further analysis (Table 1). Figures 23, 24 and 25 show the power attenuations of the transmitted waves from the normally incident plane wave with a unit power on the aperture. Only two modes (TE_{11} and TE_{12}) are propagating in this particular geometry (Figures 2 and 3) and 84% of the incident power on the aperture is transmitted in this approximation. There are two interesting features to be observed. Most of the power is carried by the dominant mode (TE_{11})(which has been discussed in Section 2.3) and the attenuation constant of the dominant mode is usually larger than that of the higher mode. As those two modes propagate through the waveguide, eventually the higher mode will carry most of the power, but when this happens, the total power of the wave has already decayed to a small fraction of the initial transmitted power at $z = 0$.

TABLE 1.

THE DIELECTRIC CONSTANTS OF THE LOSSY DIELECTRIC MATERIALS AND THE PROPAGATION CONSTANTS OF TE_{11} AND TE_{12} MODES WHEN THESE MATERIALS ARE USED IN THE WAVEGUIDE (a = 9.7 cm, b = 10 cm, f = 3 GHz (b/λ = 1))

Figure	23	24	25
Material	Polystyrene 7%	Catalin 700 base	Pyralin
*Real ε_r	9.1	4.74	3.74
*Imag ε_r	-2.275	-0.7252	-0.6171
Real $k_z \times b$ TE_{11}	6.1321	6.1059	6.0960
Imag $k_z \times b$ TE_{11}	-1.0388×10^{-2}	-6.1856×10^{-3}	-7.2436×10^{-3}
Real $k_z \times b$ TE_{12}	3.3726	3.3554	3.3513
Imag $k_z \times b$ TE_{12}	-9.2734×10^{-3}	-2.9211×10^{-3}	-2.6319×10^{-3}

*Reference (8)

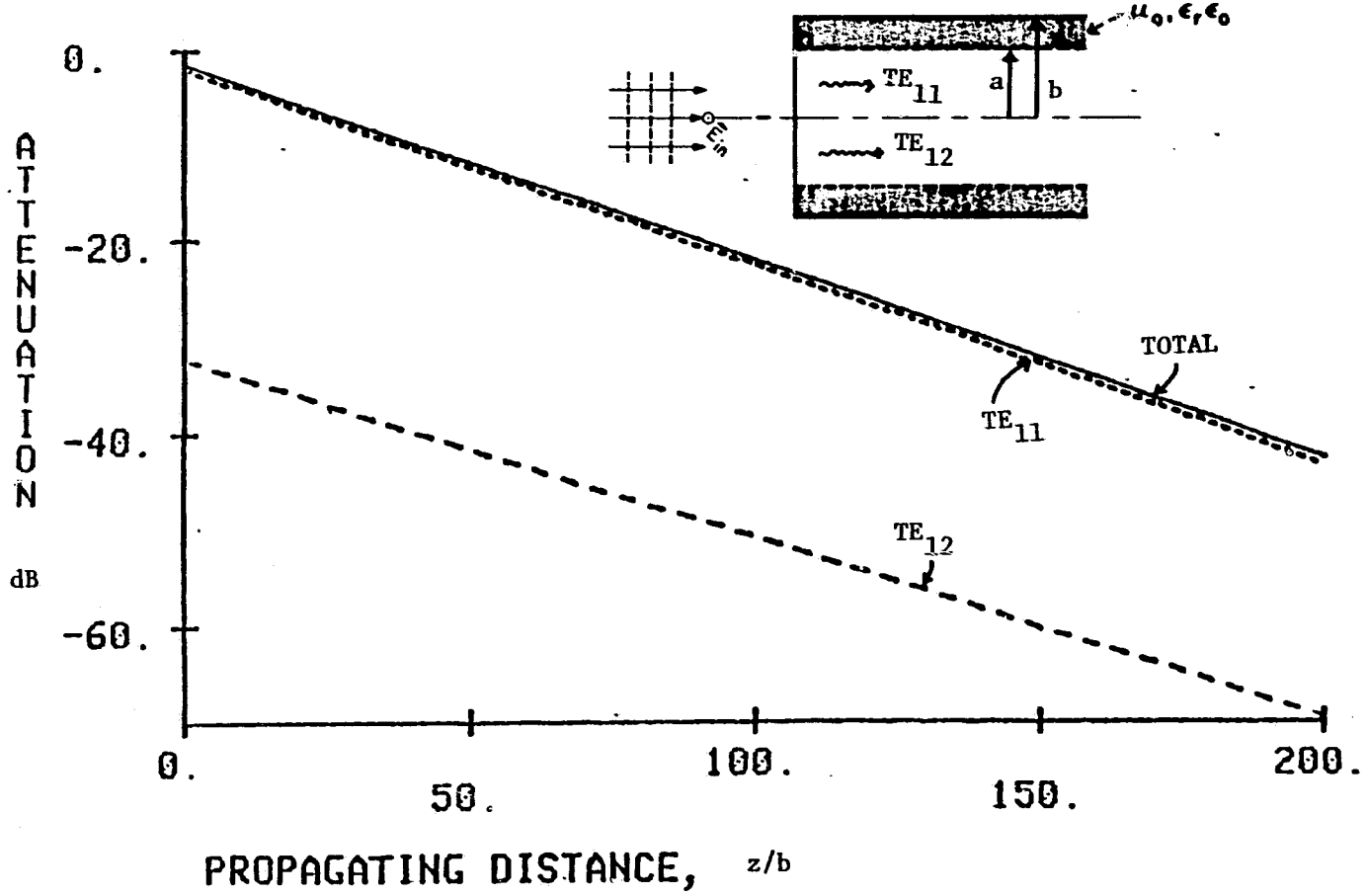

Figure 23. Attenuation along the waveguide for a normally incident plane wave (polystyrene 70% and carbon 30% (ε_r = 9.1 - j2.28), a = 9.7 cm, b = 10 cm, f = 3 GHz).

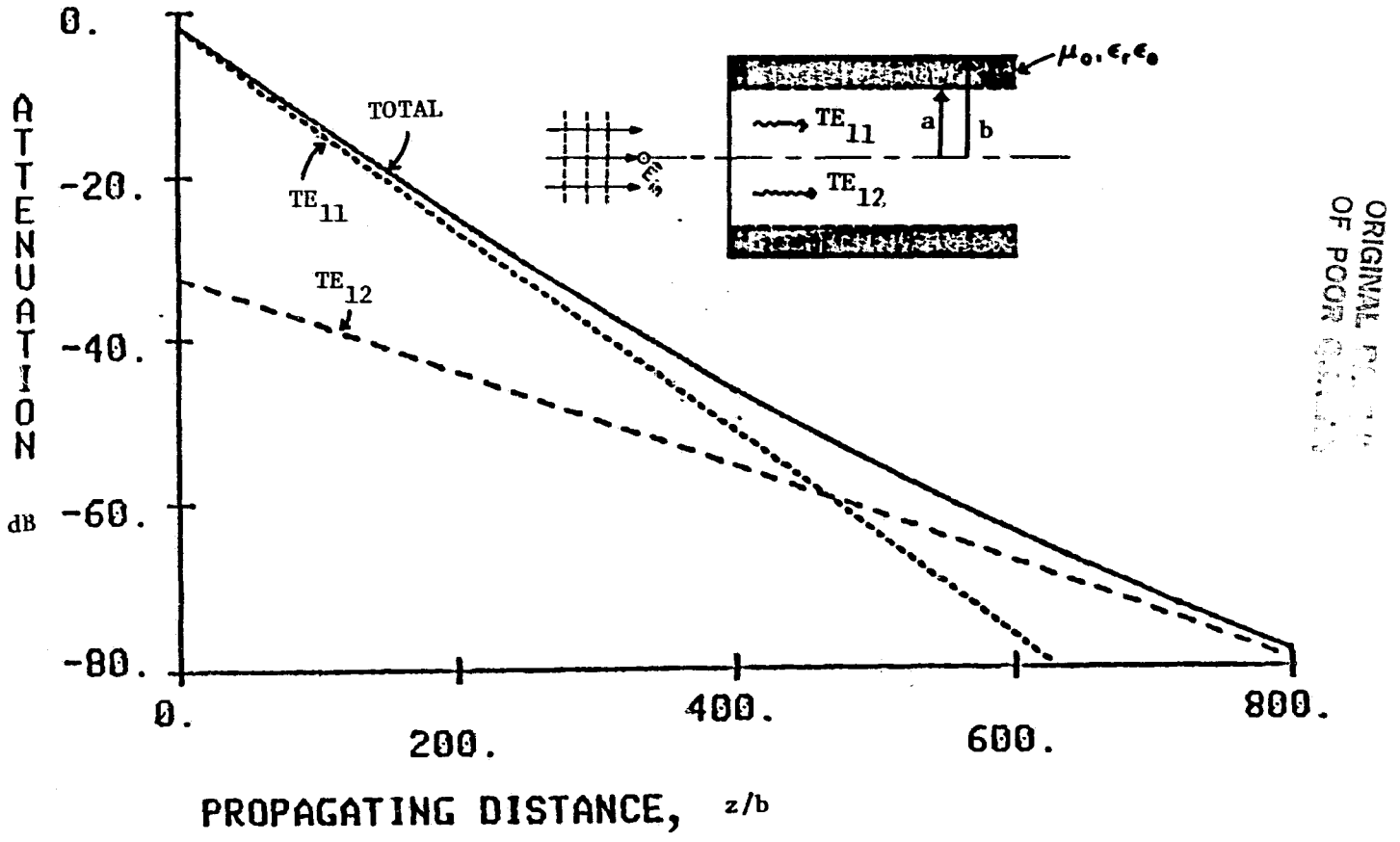

Figure 24. Attenuation along the waveguide for a normally incident plane wave (catalin 700 base (ε_r = 4.74 - j0.73), a = 9.7 cm, b = 10 cm, f = 3 GHz).

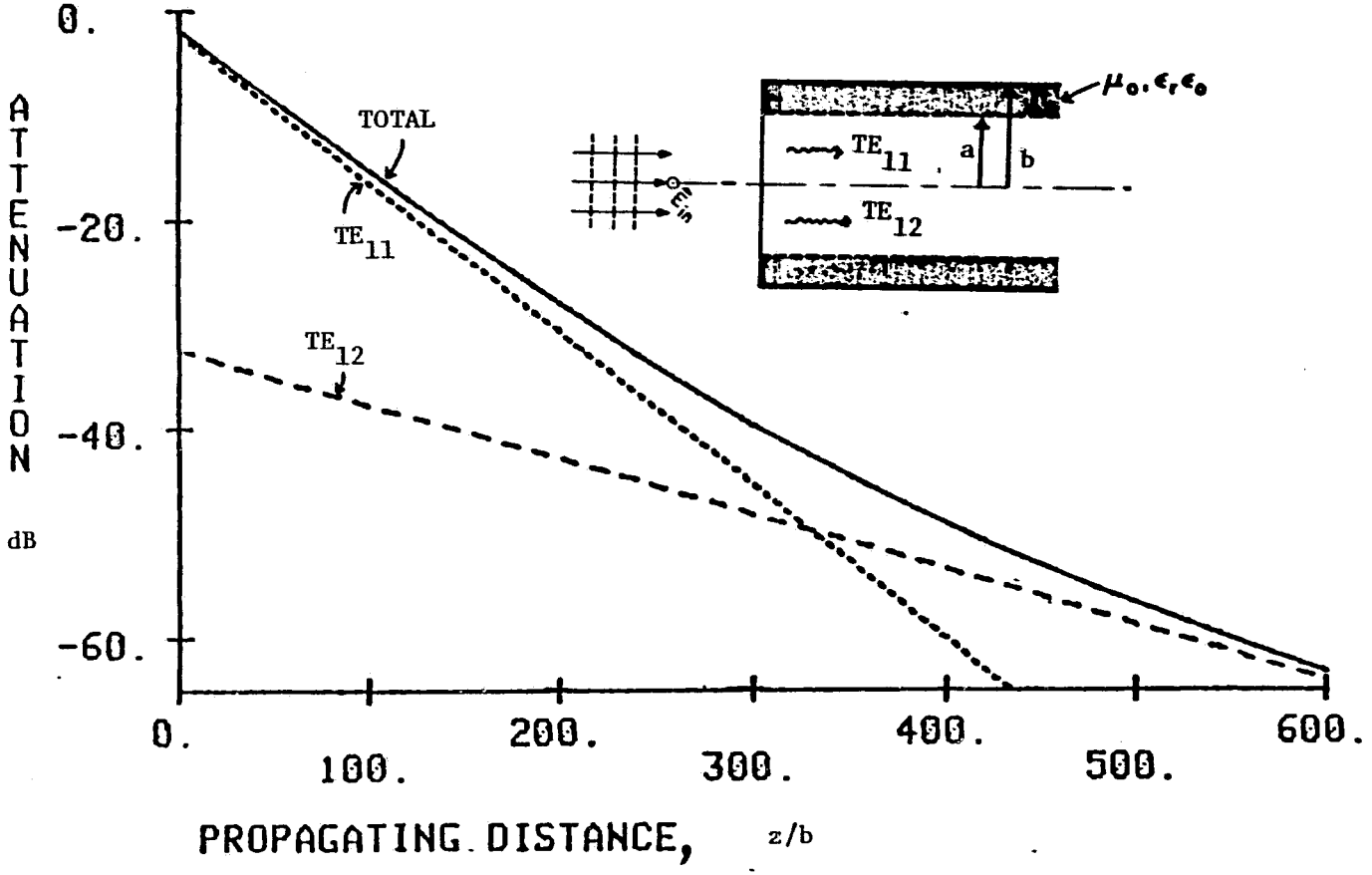

Figure 25. Attenuation along the waveguide for a normally incident plane wave (pyralin (ϵ_r = 3.74 - j0.62), a 9.7 cm, b = 10 cm, f = 3 GHz).

4. CONCLUSION AND DISCUSSION

We have calculated the attenuation constants of the normal modes in the waveguide coated with a lossy dielectric material. When the lossy-dielectric layer is thin, choosing the dielectric material with a large loss tangent results in a large attenuation constant of the normal mode (TE or TM). We have chosen a few practical materials for the lossy dielectric to demonstrate the power attenuation of the wave in the lossy waveguide from the normally incident plane wave. Unfortunately, the power attenuation may not be sufficient in a practical application. For a circular waveguide coated with the thin layer ($(b - a)/b = 3\%$) of the best dielectric material available (polystyrene 70% and carbon 30%, $\varepsilon_r = 9.1 - j2.3$), a 3 dB attenuation can be achieved around a distance of 16 diameters.

We have also calculated the attenuation constant as a function of the thickness of the lossy dielectric layer. There may exist an optimum thickness of the lossy dielectric layer for large attenuation, and the behavior of the attenuation constants of the TE and TM modes as a function of the dielectric constant of the lossy material are different from that in the thin-layer case. That is, choosing the lossy material with a smaller ε_r^I results in a larger attenuation constant for the TE mode but a smaller attenuation constant for the TM mode, or vice versa. Usually, TE modes attenuate more than TM modes in the thicker layer case.

The main reason we can not obtain a large attenuation constant in the waveguide coated with a thin lossy dielectric layer is that the electric field $|\vec{E}|$ is small because its tangential component vanishes at the perfectly conducting surface and its normal component is inversely proportional to the dielectric constant, which is usually large for the available materials. A thick lossy

dielectric layer may be used for a large attenuation constant of the normal mode. For example, when the waveguide is coated with the thick dielectric layer ((b - a)/b = 10%) of Catalin (700 base, $\varepsilon_r = 4.7 - j0.7$), a 3 dB attenuation can be obtained within a distance of one diameter. However, too thick a layer may not be desirable in the design of the structure.

It may be possible to attain a large attenuation constant of the normal mode even with a thin dielectric layer but with a different pattern of coating. Consider a waveguide which is coated with double layers (Figure 26a). If we use the dielectric with a large dielectric constant for the outer layer, then the modal field will shift to the surface, and the electric field in the inner dielectric layer with a large ε_r^I will be large, where the power of the wave is dissipated. We have seen in Section 3.1.2 that the tangential field does not contribute much to the power dissipation in the case of a single thin dielectric layer. Increasing the tangential component of the electric field with a multilayer coating makes this component play a major role in the power dissipation of the guided wave. The above effect with the multilayer can be achieved with commercially available resistive sheets (Figure 26b).

Another way by which the electric field in the dielectric region can be increased may be using the corrugated layers (Figure 27a). The basic idea in this device is to increase the radial component of the electric field in the dielectric region by making space within the dielectric layer.

Since the electric field at the center region is usually large, it has been suggested that putting the lossy material (e.g., resistive cards) at the center region may increase the attenuation constant (Figure 27b).

The feasibility of those devices mentioned above also depends on the actual design problem of the jet intake.

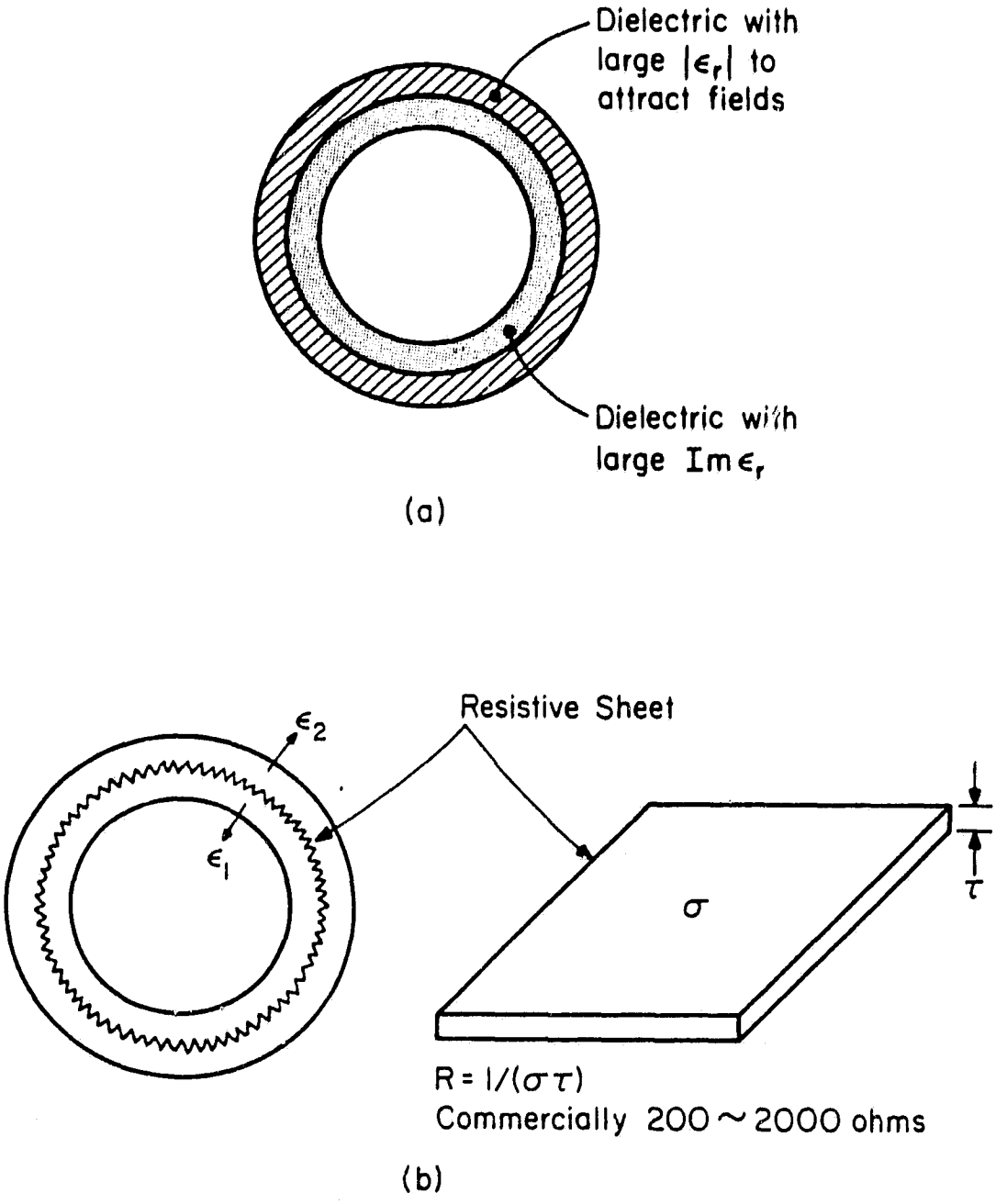

Figure 26. Multilayer structures: a) double layers, b) resistive sheet.

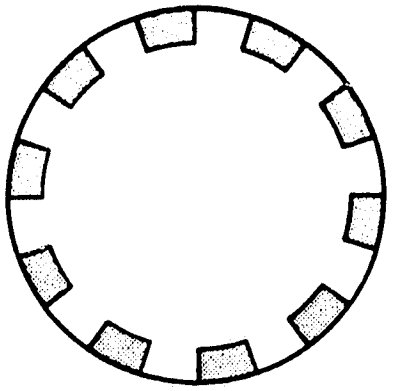

(a)

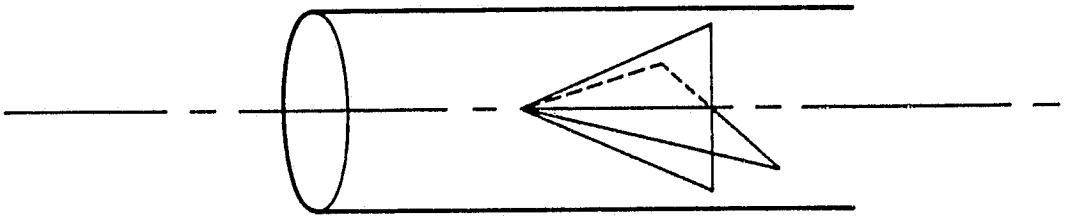

(b)

Figure 27. Other possible devices for a large attenuation constant: a) corrugated layer, b) resistive card.

APPENDIX 1

APPROXIMATE SOLUTION OF THE PROPAGATION CONSTANT IN THE CYLINDRICAL WAVEGUIDE COATED WITH A LOSSY DIELECTRIC MATERIAL

In this appendix, we derive the approximate solution based on the perturbation theory. Refer to the main text for the notations.

The fields in the perfect cylindrical waveguide are given by

$\vec{A} = \hat{z}\bar{\psi}$ (magnetic vector potential)

$$\bar{E}_\rho = \frac{1}{j\omega\epsilon}\frac{\partial^2\bar{\psi}}{\partial\rho\partial z} \quad , \quad \bar{H}_\rho = \frac{1}{\rho}\frac{\partial\bar{\psi}}{\partial\phi}$$

$$\bar{E}_\phi = \frac{1}{j\omega\epsilon\rho}\frac{\partial^2\bar{\psi}}{\partial\phi\partial z} \quad , \quad \bar{H}_\phi = -\frac{\partial\bar{\psi}}{\partial\rho}$$

$$\bar{E}_z = \frac{1}{j\omega\epsilon}\left(\frac{\partial^2}{\partial z^2} + k^2\right)\bar{\psi} \quad , \quad \bar{H}_z = 0 \qquad \text{for TM} \qquad \text{(A1.1)}$$

and

$\vec{F} = \hat{z}\psi$ (electric vector potential)

$$E_\rho = -\frac{1}{\rho}\frac{\partial\psi}{\partial\phi} \quad , \quad H_\rho = \frac{1}{j\omega\mu}\frac{\partial^2\psi}{\partial\rho\partial z}$$

$$E_\phi = \frac{\partial\psi}{\partial\rho} \quad , \quad H_\phi = \frac{1}{j\omega\mu\rho}\frac{\partial^2\psi}{\partial\phi\partial z}$$

$$E_z = 0 \quad , \quad H_z = \frac{1}{j\omega\mu}\left(\frac{\partial^2}{\partial z^2} + k^2\right)\psi \qquad \text{for TE} \qquad \text{(A1.2)}$$

The wave functions satisfying the boundary condition are

$$\overline{\psi}_{mn} = J_m\left(\frac{\xi_{mn}}{b}\rho\right)\begin{bmatrix}\cos m\phi\\ \sin m\phi\end{bmatrix} e^{-jk_z z} \tag{A1.3}$$

$$\psi_{mn} = J_m\left(\frac{\xi'_{mn}}{b}\rho\right)\begin{bmatrix}\cos m\phi\\ \sin m\phi\end{bmatrix} e^{-jk_z z} \tag{A1.4}$$

where ξ_{mn} and ξ'_{mn} are n^{th} zeros of $J_n(x)$ and $J'_n(x)$, respectively. The dispersion relation is

$$k_z^2 + k_\rho^2 = k_o^2 \equiv \omega^2 \mu_o \varepsilon_o \tag{A1.5}$$

where

$$k_\rho = \frac{\xi_{mn}}{b} \text{ or } \frac{\xi'_{mn}}{b} \tag{A1.6}$$

We approximate the perturbed fields in the denominator of Eq. (2.1) by the unperturbed fields. In the numerator, we use the quasistatic approximation [5] such that

$$\vec{E} \simeq \frac{1}{\varepsilon_r}\vec{E}_o \tag{A1.7}$$

where ε_r is the complex dielectric constant of the coating material. This may be a good approximation assuming the tangential electric field is small near the surface and the electric field is nearly normal to the surface in the dielectric region. Assuming $\Delta\mu = 0$, Eq. (2.1) becomes in this approximation

$$k_z - k_{zo} = -\frac{\omega\varepsilon_o \int_{d.r.} (\varepsilon_r - 1)\,\vec{E}_o \cdot \vec{E}_o \, dS}{2\int_S (\vec{E}_o \times \vec{H}_o)\cdot\hat{z}\, dS} \tag{A1.8}$$

where the integral in the numerator is over the cross section in the dielectric region (d.r.), and the one in the denominator is over the cross-sectional area of the cylinder.

Substituting the fields for the TE mode in (A1.2), we obtain

$$k_z - k_{zo} = -\frac{\omega^2 \mu_o \varepsilon_o (\varepsilon_r - 1)}{2 \varepsilon_r k_{zo}} \frac{\int_{\frac{a}{b}\xi'_{mn}}^{\xi'_{mn}} g_m(x)\, dx}{\int_0^{\xi_{mn}} g_m(x)\, x dx} \quad \text{for } HE_{mn} \ (TE_{mn}) \tag{A1.9}$$

where

$$g_m(x) = \frac{n^2}{x^2} J_m^2(x) + J_m'^2(x) \ . \tag{A1.10}$$

Using the recurrence formula [9],

$$g_m(x) = J_{m+1}^2(x) + \frac{m}{x} \frac{d}{dx} J_m^2(x) \tag{A1.11}$$

Substituting Eq. (A1.11) in Eq. (A1.9), we obtain

$$k_z - k_{zo} = \frac{\omega^2 \mu_o \varepsilon_o (\varepsilon_r - 1)}{2 \varepsilon_r k_{zo}} \left\{ 1 - \frac{f\left(\frac{\xi'_{mn} a}{b}\right)}{\frac{(\xi'_{mn})^2 - n^2}{2} J_m^2(\xi'_{mn})} \right\} \text{for } HE_{mn}(TE_{mn}) \tag{2.2}$$

where f(x) is given in Eq. (2.4). For the TM mode, we follow a similar procedure with the fields given in Eqs. (A1.1) and (A1.3). Then we obtain

$$k_z - k_{zo} = \frac{k_{zo}(\varepsilon_r - 1)}{\varepsilon_r} \left\{ 1 - \frac{\left[f\frac{\xi_{mn} a}{b} \right]}{\frac{\xi_{mn}^2}{2} J_{m+1}^2(\xi_{mn})} \right\} \quad \text{for } EH_{mn} \ (TM_{mn}) \tag{2.3}$$

APPENDIX 2

EXACT NUMERICAL SOLUTION OF THE PROPAGATION CONSTANT IN THE CYLINDRICAL WAVEGUIDE COATED WITH A LOSSY DIELECTRIC MATERIAL [10]

The field expressions in terms of the wave functions are given in Appendix 1. The wave functions in Region I (Figure 1) satisfying the boundary condition at the origin are given by

$$\bar{\psi}_m^I(k_{\rho 1}\rho) = AJ_m(k_{\rho 1}\rho)\cos m\phi\, e^{-jk_z z} \tag{A2.1}$$

$$\psi_m^I(k_{\rho 1}\rho) = BJ_m(k_{\rho 1}\rho)\sin m\phi\, e^{-jk_z z} \tag{A2.2}$$

and the wave functions in Region II satisfying the boundary condition at the conducting surface are given by

$$\bar{\psi}_m^{II}(k_{\rho 2}\rho) = C[J_m(k_{\rho 2}\rho)\, N_m(k_{\rho 2}b) - N_m(k_{\rho 2}\rho)\, J_m(k_{\rho 2}b)]\cos m\phi\, e^{-jk_z z} \tag{A2.3}$$

$$\psi_m^{II}(k_{\rho 2}\rho) = D[J_m(k_{\rho 2}\rho)\, N_m'(k_{\rho 2}b) - N_m(k_{\rho 2}\rho)\, J_m'(k_{\rho 2}b)]\sin m\phi\, e^{-jk_z z} \tag{A2.4}$$

where

$$\begin{aligned} k_{\rho 1}^2 + k_z^2 &= \omega^2\varepsilon_1\mu_1 = k_1^2 \\ k_{\rho 2}^2 + k_z^2 &= \omega^2\varepsilon_2\mu_2 = k_2^2 \end{aligned} \tag{A2.5}$$

ψ's with and without the bar indicate TM and TE modes, respectively. For other notations, please refer to the main text (Section 2.1). Note that the angular terms of the wave functions are chosen such that these two modes are coupled.

Substituting Eqs. (A2.1) through (A2.4) in Eqs. (A1.1) and (A1.2), we obtain the general field expressions given in Eqs. (2.13) through (2.18). Matching the tangential fields between Regions I and II, we have four equations,

$$E_z: \quad A\frac{k_{\rho 1}^2 F_1}{\varepsilon_1} = C\frac{k_{\rho 2}^2 F_3}{\varepsilon_2}$$

$$H_z: \quad B\frac{k_{\rho 1}^2 F_1}{\mu_1} = D\frac{k_{\rho 2}^2 F_4}{\mu_2}$$

$$H_\phi: \quad Ak_{\rho 1}F_1' + \frac{Bk_z m}{\omega\mu_1 a}F_1 = Ck_{\rho 2}F_3' + \frac{Dk_z m}{\omega\mu_2 a}F_4$$

$$E_\phi: \quad \frac{Ak_z m}{\omega\varepsilon_1 a}F_1 + Bk_{\rho 1}F_1' = \frac{Ck_z m}{\omega\varepsilon_2 a}F_3 + Dk_{\rho 2}F_4' \qquad \text{(A2.6)}$$

where the notations are given in Section 2.1.2. For a nontrivial solution for A, B, C and D, the determinant for Eq. (A2.6) must vanish. This condition gives the characteristic equation given in Eq. (2.5).

APPENDIX 3

NORMAL MODES PROPAGATING INTO A CYLINDRICAL WAVEGUIDE FROM THE INCIDENT PLANE WAVE

The geometry for this problem is shown in Figure 2, and the notations are indicated in the main text (Section 2.3).

The transverse electric and magnetic fields in the waveguide at $z = 0^+$ are given by

$$\vec{E}_t(z = 0^+) = \sum_{m,n}\left[C^V_{mn}\vec{U}^V_{mn} + C^H_{mn}\vec{U}^H_{mn} + \frac{\overline{k}_{zmn}}{k_o}\overline{C}^V_{mn}\overline{V}^V_{mn} + \frac{\overline{k}_{zmn}}{k_o}\overline{C}^H_{mn}\overline{V}^H_{mn}\right] \tag{A3.1}$$

$$\vec{H}_t(z = 0^+) = \frac{1}{Z_o}\sum_{m,n}\left[\frac{k_{zmn}}{k_o}C^V_{mn}(\hat{z} \times \vec{U}^V_{mn}) + \frac{k_{zmn}}{k_o}C^H_{mn}(\hat{z} \times \vec{U}_{mn}) + \overline{C}^V_{mn}(\hat{z} \times \vec{V}^V_{mn}) + \overline{C}^H_{mn}(\hat{z} \times \vec{V}^H_{mn})\right] \tag{A3.2}$$

where C's are constants. The symbols with the bar indicate the TM mode, while those without the bar indicate the TE mode, and $\vec{U}$ and $\vec{V}$ are given in Eqs. (2.26) and (2.27). We can also write $\vec{U}$ and $\vec{V}$ such that

$$\vec{U}^{V,H}_{mn} = N_{mn}\,\hat{z} \times \nabla_t \psi^{V,H}_{mn} \tag{A3.3}$$

$$\vec{V}^{V,H}_{mn} = -\overline{N}_{mn}\,\nabla_t \overline{\psi}^{V,H}_{mn} \tag{A3.4}$$

where

$$\begin{bmatrix}\psi^V_{mn}\\ \psi^H_{mn}\end{bmatrix} = J_m\left(\frac{\xi'_{mn}}{b}\rho\right)\begin{bmatrix}\cos m\phi\\ \sin m\phi\end{bmatrix} \tag{A3.5}$$

$$\begin{bmatrix}\overline{\psi}^V_{mn}\\ \overline{\psi}^H_{mn}\end{bmatrix} = J_m\left(\frac{\xi_{mn}}{b}\rho\right)\begin{bmatrix}\sin m\phi\\ \cos m\phi\end{bmatrix} \tag{A3.6}$$

Define the orthonormalization condition such that

$$\langle \vec{U}^{V,H}_{mn} \cdot \vec{U}^{V,H}_{m'n'} \rangle = Z_o \delta_{mm'} \delta_{nn'} \tag{A3.7a}$$

$$\langle \vec{V}^{V,H}_{mn} \cdot \vec{V}^{V,H}_{m'n'} \rangle = Z_o \delta_{mm'} \delta_{nn'} \tag{A3.7b}$$

$$\langle \vec{U}^{V,H}_{mn} \cdot \vec{V}^{V,H}_{m'n'} \rangle = 0 \tag{A3.7c}$$

Superscripts V, H indicate that these conditions apply to both cases of vertical and horizontal polarizations. However these two normal fields are orthogonal. Substituting Eq. (A3.3) in the right-hand side of Eq. (A3.7a), we obtain

$$\begin{aligned}
\langle \vec{U}^{V,H}_{mn} \cdot \vec{U}^{V,H}_{m'n'} \rangle &= N^2_{mn} \langle (\hat{z} \times \nabla_t \psi^{V,H}_{mn}) \cdot (\hat{z} \times \nabla_t \psi^{V,H}_{m'n'}) \rangle \\
&= N^2_{mn} \langle \nabla_t \psi^{V,H}_{mn} \cdot \nabla_t \psi^{V,H}_{m'n'} \rangle \\
&= N^2_{mn} \iint_S \nabla_t \psi^{V,H}_{mn} \cdot \nabla_t \psi^{V,H}_{m'n'} \, dS \\
&= -N^2_{mn} \iint_S \psi^{V,H}_{mn} \nabla^2_t \psi^{V,H}_{m'n'} \, dS + \oint_c \psi^{V,H}_{mn} \frac{\partial \psi^{V,H}_{mn}}{\partial \rho} \, d\ell
\end{aligned} \tag{A3.8}$$

Due to the boundary condition at the surface, the second term vanishes. Since

$$\nabla^2_t \psi^{V,H}_{m'n'} = -\left(\frac{\xi_{m'n'}}{b}\right)^2 \psi^{V,H}_{m'n'} ,$$

(A3.8) becomes

$$\langle \vec{U}^{V,H}_{mn} \cdot \vec{U}^{V,H}_{mn} \rangle = N^2_{mn} \delta_{mm'} \delta_{nn'} (1 + \delta_{m0}) \, \pi \left(\frac{\xi'_{mn}}{b}\right)^2 \int_0^b \rho d\rho \left[J_m\left(\frac{\xi'_{mn}}{b}\right)\rho \right]^2$$

$$= N^2_{mn} \delta_{mm'} \delta_{nn'} (1 + \delta_{m0}) \frac{\pi}{2} J^2_m(\xi'_{mn}) [(\xi'_{mn})^2 - m^2]$$

Then, the normalization constant becomes

$$N_{mn} = [2Z_o/\pi(1 + \delta_{m0})]^{1/2} \; [(\xi'_{mn})^2 - m^2]^{-1/2} \; |J_m(\xi'_{mn})|^{-1} \tag{A3.9}$$

Equations (A3.7b) and (A3.7c) can be similarly proved. The normalization constant of the TM mode is shown to be

$$\overline{N}_{mn} = [2Z_o/\pi(1 + \delta_{m0})]^{1/2} \; |\xi_{mn} J_{m+1}(\xi_{mn})|^{-1} \tag{A3.10}$$

First, we assume the tangential electric field is continuous at $z = 0$:

$$\vec{E}_t^{in}(z = 0^-) = \vec{E}_t(z = 0^+) \tag{A3.11}$$

From Eq. (2.22),

$$\vec{E}_t^{in}(z = 0^-) = E_o \, \hat{x} \cos \theta_o \exp[-jk_x x] \tag{A3.12}$$

and the right-hand side of Eq. (A3.11) is given in Eq. (A3.1). Multiplying both sides of Eq. (A3.12) by the integration operator,

$$\int_o^b \rho d\rho \int_o^{2\pi} d\phi \; \vec{U}_{mn}^{V,H} \cdot \tag{A3.13}$$

and using the orthonormalization conditions of Eq. (3.7), we obtain

$$Z_o \begin{bmatrix} C_{mn}^V \\ C_{mn}^H \end{bmatrix} = E_o \cos \theta_o \int_0^b \rho d\rho \int_0^{2\pi} d\phi \begin{bmatrix} \vec{U}_{mn}^V \cdot \vec{Y}(x) \\ \vec{U}_{mn}^H \cdot \vec{Y}(x) \end{bmatrix} \tag{A3.14}$$

where

$$\vec{Y}(x) = \hat{x} \, e^{-jk_x x}$$

Amitay and Galindo evaluated the integral of Eq. (A3.14) (Eq. (6) in reference [11]). The coefficients in Eq. (A3.14) then become

$$\begin{bmatrix} C^V_{mn} \\ C^H_{mn} \end{bmatrix} = \frac{E_o}{Z_o} \cos\theta_o \, N_{mn} \frac{2\pi m}{k_x} (-j)^{m-1} J_m(\xi'_{mn}) J_m(k_x b) \begin{bmatrix} 0 \\ -1 \end{bmatrix} \tag{A3.15}$$

We can following a similar procedure for the other two coefficients. They are shown to be

$$\begin{bmatrix} \bar{C}^V_{mn} \\ \bar{C}^H_{mn} \end{bmatrix} = \frac{E_o k_o}{Z_o k_{zmn}} \cos\theta_o \, \bar{N}_{mn} \frac{2\pi\xi_{mn}(-j)^{m-1}}{k_x^2 - \left(\frac{\xi_{mn}}{b}\right)^2} k_x J'_m(\xi_{mn}) J_m(k_x b) \begin{bmatrix} 0 \\ -1 \end{bmatrix} \tag{A3.16}$$

If we match the tangential magnetic field,

$$\bar{H}^{in}_t(z = 0^-) = \bar{H}_t(z = 0^+) \tag{A3.17}$$

where

$$\bar{H}^{in}_t(z = 0^+) = \frac{E_o}{Z_o} \hat{y} \, e^{-jk_x x}$$

and the right-hand side of Eq. (A3.17) is given in Eq. (A3.2). If we follow a similar procedure as before, the result is different from the one obtained by matching the tangential electric fields. The only difference in this case is that the cos θ_o terms in Eqs. (A3.15) and (A3.16) and the factor of k_{zmn}/k_o. The coefficients in this approach is given by

$$\begin{bmatrix} C^V_{mn} \\ C^H_{mn} \end{bmatrix} = \frac{E_o k_o}{z_o k_{zmn}} N_{mn} \frac{2\pi m}{k_x} (-j)^{m-1} J_m(\xi'_{mn}) J_m(k_x b) \begin{bmatrix} 0 \\ -1 \end{bmatrix} \tag{A3.18}$$

$$\begin{bmatrix} \overline{C}^{V}_{mn} \\ \overline{C}^{H}_{mn} \end{bmatrix} = \frac{E_o}{Z_o} \overline{N}_m \frac{2\pi\xi_{mn}(-j)^{m-1}}{k_x - \left(\frac{\xi_{mn}}{b}\right)^2} k_x J_m'(\xi_{mn}) J_m(k_x b) \begin{bmatrix} 0 \\ -1 \end{bmatrix} \tag{A3.19}$$

In this report, we use the electrical-field matching. Witt and Price [12] indicated that using the magnetic-field matching gives a better convergency for the high (evanescent) modes. However, as shown in Eq. (A.18), this method gives a very large coefficient for the mode near the cutoff frequency. In this case, the total power transmitted may be more than 100%, which can not be justified in a physical point of view.

When $\theta_o = 0$ (normal incidence), matching the electric fields at $z = 0$, the transmitted tangential electric field is given by

$$\vec{E}_t = 2E_o \sum_n \frac{e^{-jk_{z1n}z}}{J_1(\xi'_{1n})[(\xi'_{1n})^2 - 1]} \left[\hat{\rho} \frac{b}{\rho} J_1\left(\frac{\xi'_{1n}}{b}\rho\right) \cos\phi - \hat{\phi}\, \xi'_{1n} J_1'\left(\frac{\xi'_{1n}}{b}\rho\right) \sin\phi \right] \tag{A3.20}$$

Note that we have terms with $m = 1$ only because the incident field is linearly polarized in the $\hat{x}$-direction. Also, from Eq. (A3.2), the transverse magnetic field is given by

$$\vec{H}_t = -\frac{2E_o}{Z_o k_o} \sum_n \frac{e^{-jk_{z1n}z}\, k_{z1n}}{J_1(\xi'_{1n})[(\xi'_{1n})^2 - 1]} \left[\hat{\rho}\, \xi'_{1n} J_1'\left(\frac{\xi'_{1n}}{b}\rho\right) \sin\phi + \hat{\phi} \frac{b}{\rho} J_1\left(\frac{\xi'_{1n}}{b}\rho\right) \cos\phi \right] \tag{A3.21}$$

Assuming that the perturbation is not too large, we use the fields in the

unperturbed waveguide for the fields in the perturbed waveguide except for the exponentially decaying factor in the z-direction. Then the power attenuation of the transmitted wave from the normally incident field is given by

$$\frac{P}{P_o} = \frac{4}{b^2 k_o} \sum_n \frac{\beta_{1n} \exp[-2z\alpha_{1n}]}{[J_1(\xi'_{1n})((\xi'_{1n})^2 - 1)]^2}$$

$$\times \int_0^b \rho d\rho \left[\frac{b^2}{\rho^2} \left\{ J_1\left(\frac{\xi'_{1n}}{b} \rho \right) \right\}^2 + \xi_{1n}^2 \left\{ J_1'\left(\frac{\xi'_{1n}}{b} \rho \right) \right\}^2 \right]$$

$$= 2 \sum \frac{(\beta_{in}/k_o) \exp[-2z\alpha_{1n}]}{(\xi'_{1n})^2 - 1} \qquad \text{(A3.22)}$$

where

$$k_{z1n} = \beta_{1n} - j\alpha_{1n}$$

$$P_o = E_o^2 \pi b^2 / Z_o$$

Here P_o is the power incident on the area of the aperture. The integration in Eq. (A3.22) is evaluated in Eq. (A1.9).

REFERENCES

[1] S. W. Lee and Y. T. Lo, "Electromagnetic scattering by cylinder and sphere," Electromagnetics Laboratory Report No. 83-1, University of Illinois, Urbana, Illinois, 1983.

[2] T. W. Johnson and D. L. Moffatt, "Electromagnetic scattering by open circular waveguides," Technical Report 710816-9, Electro-Science Laboratory, Department of Electrical Engineering, The Ohio State University, Columbus, Ohio 43212, December 1980 and references therein.

[3] G. N. Tsandoulas and W. J. Ince, "Modal inversion in circular waveguides - Part I: Theory and phenomenology," IEEE Trans. Microwave Theory Tech., vol. MTT-19, pp. 386-392, April 1971.

[4] P. J. B. Clarricoats, "Propagation along unbounded and bounded dielectric rods," part 1 and part 2, Proc. Inst. Elect. Eng., Mon. 409E and 410E, pp. 170-186, October 1960.

[5] R. F. Harrington, Time Harmonic Electromagnetic Fields. New York: McGraw-Hill Book Co; 1961, Ch. 7.

[6] L. A. Weinstein, The Theory of Diffraction and the Factorization Method. Boulder, Colorado: The Golem Press, 1969.

[7] C. A. Chuang, C. S. Liang, and S. W. Lee, "High-frequency scattering from an open-ended semi-infinite cylinder," IEEE Trans. Antenna Propagat., vol. AP-23(6), pp. 770-776, November 1975.

[8] A. R. Von Hippel, ed., Dielectric Materials and Applications. Cambridge, Massachusetts: Technology Press, M.I.T., 1954.

[9] M. Abramowitz and I. A. Stegun, Handbook of Mathematical Functions. New York: Dover, 1972.

[10] Reference 5, Chapter 5.

[11] N. Amitay and V. Galindo, "On the scalar product of certain circular and Cartesian wave functions," IEEE Trans. Microwave Theory Tech., vol. MTT-16, pp. 265-266, April 1968.

[12] H. R. Witt and E. L. Price, "Scattering from hollow conducting cylinders," Proc. IEE, vol. 115, no. 1, pp. 94-99, January 1968.